

Generation of T cells with reduced off-target cross-reactivities by engineering co-signalling receptors

Jose Cabezas-Caballero¹, Anna Huhn¹, Mikhail A. Kutuzov¹, Violaine Andre¹, Alina Shomuradova¹

P. Anton van der Merwe¹, Omer Dushek^{1,¶}

¹Sir William Dunn School of Pathology, University of Oxford, Oxford OX1 3RE, UK

¶Corresponding author

One sentence summary: Switching the CD8 for the CD4 co-receptor in cytotoxic T cells reduces the functional cross-reactivity of T cells without modifying the TCR.

Key words: Adoptive cell therapy; T cell receptor; T cell cross-reactivity; Antigen discrimination; Antigen affinity; Co-signalling receptors;

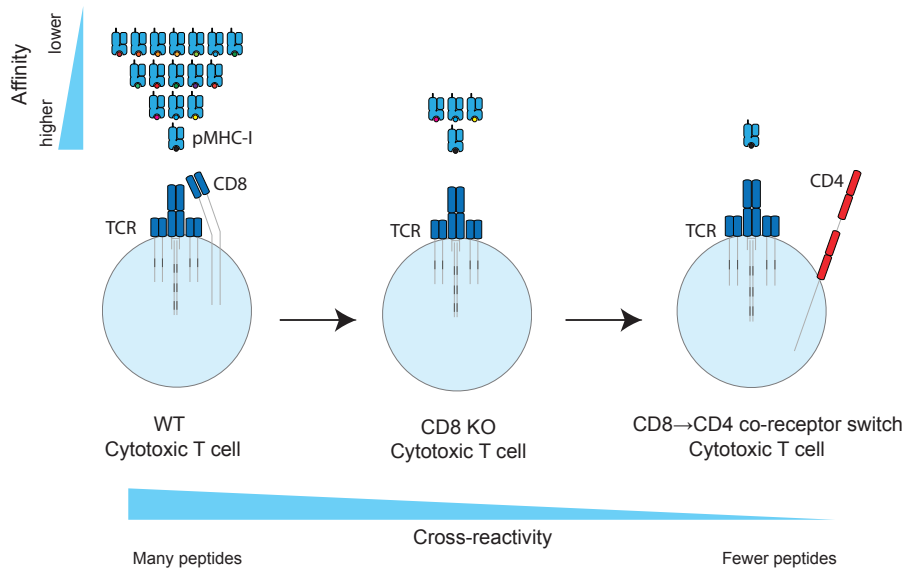
Pre-print server: <https://www.biorxiv.org>

Open access: This research was funded in whole, or in part, by the Wellcome Trust [207537/Z/17/Z]. For the purpose of Open Access, the authors have applied a CC BY public copyright licence to any Author Accepted Manuscript version arising from this submission.

Abstract:

Adoptive T cell therapy using T cells engineered with novel T cell receptors (TCRs) targeting tumor-specific peptides is a promising immunotherapy. However, these TCR-T cells can cross-react with off-target peptides, leading to severe autoimmune toxicities. Current efforts focus on identifying TCRs with reduced cross-reactivity. Here, we show that T cell cross-reactivity can be controlled by the co-signalling molecules CD5, CD8, and CD4, without modifying the TCR. We find the largest reduction in cytotoxic T cell cross-reactivity by knocking out CD8 and expressing CD4. Cytotoxic T cells engineered with a CD8-to-CD4 co-receptor switch show reduced cross-reactivity to random and positional scanning peptide libraries, as well as to self-peptides, while maintaining their on-target potency. Therefore, co-receptor switching generates super selective T cells that reduce the risk of lethal off-target cross-reactivity, and offers a universal method to enhance the safety of T cell immunotherapies for any TCR.

Graphical abstract



1 Introduction

2 A promising immunotherapy approach is the adoptive transfer of T cells engineered with novel T cell re-
3 ceptors (TCR-T) recognising tumour peptide antigens displayed on major histocompatibility complexes
4 (pMHCs) (1). This therapeutic strategy enables targeting nearly all tumour antigens, including tumour spe-
5 cific developmental antigens and neo-antigens (2). However, the engineered T cells can cross-react with
6 off-target peptides in healthy tissues and cause fatal autoimmune toxicities (3–5). This cross-reactivity has
7 hampered efforts to produce highly potent TCR-T cell therapies (6, 7).

8 Identifying the potential off-target cross-reactivities of TCRs before first-in-human clinical trials is chal-
9 lenging due to the lack of animal models or cell lines that represent the entire human proteome and HLA
10 allele diversity. Indeed, the clinical a3a TCR targeting the cancer-testis antigen MAGE-A3 passed safety
11 screens but ultimately cross-reacted with a lower affinity off-target peptide from the cardiac protein Titin,
12 causing the death of two patients (4, 5). As a result, efforts are underway to establish pipelines to identify
13 effective yet safe TCRs (8–15). Typically, these methods screen TCRs with different complementary de-
14 termining regions (CDRs) for their ability to recognise the on-target tumour but not off-target self pMHCs
15 (16). In addition to screening methods, it has also been proposed that modifying the CDR loops to reduce
16 their flexibility or introduce catch bonds may generally increase TCR specificity (17–19). However, these
17 strategies that rely on mutating the TCR sequence to reduce cross-reactivity require prior knowledge of the
18 self antigen that causes lethal cross-reactivity and modifying the TCR sequence to reduce cross-reactivity to
19 one antigen may result in new cross-reactivities to other self antigens. Collectively, this makes it challenging
20 and costly to screen and optimise each new candidate therapeutic TCR.

21 Instead of modifying the TCR CDR loops to reduce binding cross-reactivity, we hypothesised that func-
22 tional cross-reactivity can be reduced by manipulating T cell signalling without modifying the TCR. In
23 this way, even though the TCR can bind a large number peptides, T cells would only become activated in
24 response to the few peptides that bind with high affinity. Put differently, we suggest that enhancing the abil-
25 ity of T cells to discriminate antigens based on their affinity would reduce their functional cross-reactivity.
26 Given that co-signalling receptors on the T cell surface are known to impact TCR signalling (20), we rea-
27 soned that they impact T cell cross-reactivity.

28 Here, we established a platform to quantify the impact of co-signalling receptors on T cell ligand dis-
29 crimination. While a knockout of the surface molecule CD5 decreased antigen discrimination, we found
30 that a knockout of CD8 or expression of CD4 increased it. The largest effect was observed by combining
31 CD8 knockout and CD4 expression ('co-receptor switch'). We demonstrate that a CD8→CD4 co-receptor
32 switch dramatically reduced T cell cross-reactivity to peptide libraries and self peptides. Overall, co-receptor
33 switching is a broadly applicable strategy to produce super selective T cells that minimise the risk of lethal
34 cross-reactivities without compromising on-target potency, and can be applied to any TCR.

35 Results

36 T cell co-signalling receptors differentially modulate ligand sensitivity and discrimination

37 We established a platform to quantify the contribution of different T cell co-signalling receptors to ligand
38 discrimination. We selected the NY-ESO-1 specific c259 TCR contained in the investigational TCR-T ther-

39 apy lete-cel as a model system (21). First, we measured the binding affinity of the c259 TCR to a panel
40 of 7 NY-ESO-1 peptide variants on HLA-A*02:01 by Surface Plasmon Resonance (SPR) (22) (Fig. S1,
41 Table S1). Second, we used CRISPR/Cas9 to knock-out out five co-signalling receptors in primary human
42 T cells expressing the c259 TCR that were previously suggested to impact ligand discrimination: CD8 (23),
43 CD5 (24), CD43 (25), CD2 and LFA-1 (22, 26) (Fig. 1A). Third, we co-cultured these T cells with antigen-
44 presenting-cells (APCs) pulsed with a titration of each of the 7 peptides with different affinities to the TCR
45 and assessed their ability to induce multiple measures of T cell activation (target cell killing, IFN γ secretion,
46 and 4-1BB upregulation). Finally, we quantified pMHC potency as the concentration of peptide required
47 to elicit 15% activation (P15) from WT or KO T cells. By plotting the fold-change in potency (Δ P15)
48 over affinity we could determine whether the co-signalling molecule was selectively decreasing activation to
49 lower-affinity ligands (Fig. 1B).

50 We achieved high knockout efficiency of each co-signalling receptor (Fig. S2A) enabling assessment of
51 their impact on ligand discrimination (Fig. 1C-D, S2-4). The knock-out of CD43 had no impact on activation
52 whereas the knock-out of CD2 or LFA-1 individually or in combination reduced activation for all pMHC
53 affinities to a similar extent and therefore, these molecules do not impact ligand discrimination. In contrast,
54 a knock-out of CD5 selectively improved activation against lower affinity ligands and therefore, CD5 KO
55 reduced ligand discrimination. The knockout of CD8 selectively reduced activation to lower affinity peptides
56 without impacting the higher-affinity NY-ESO-1 target antigen and therefore, CD8 KO increases ligand
57 discrimination. Since the c259 TCR is affinity-matured (27), we confirmed that CD8 KO also increased the
58 discrimination of the parental wild-type 1G4 TCR (28) (Fig. S5). Taken together, co-signalling molecules
59 can control TCR ligand discrimination and a CD8 KO in particular can selectively reduce activation to lower
60 affinity ligands without impacting potency to the higher-affinity on-target antigen.

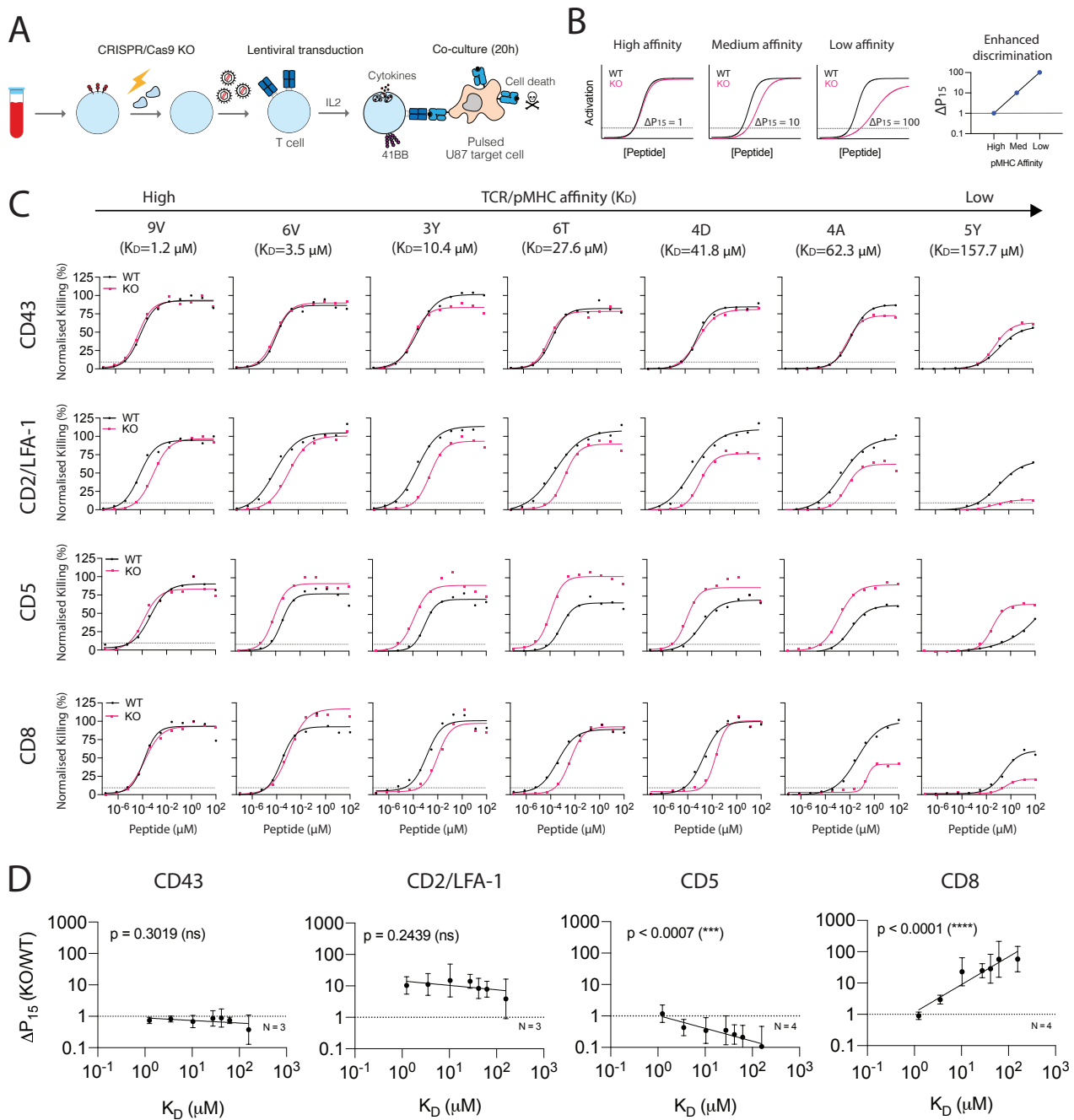


Figure 1: Measuring the impact of different T cell co-signalling receptors on ligand sensitivity and discrimination. (A) Experimental workflow to produce gene knockout primary human TCR-T cells. (B) Schematic of analysis method to determine the impact of gene knockout on ligand discrimination: changes in ligand potency between WT and KO TCR-T cells are plotted for different ligand affinities. Ligand potency (P_{15}) is the ligand concentration required to activate 15% of maximum response. (C) U87 cells were titrated with each of the 7 NY-ESO-1 peptides to stimulate WT or KO c259 TCR-T cells. Killing of the target U87 cells was measured after 20 hours. Dashed line indicates potency (P_{15}). (D) Fold change in potency (P_{15}) between KO and WT T cells from (C) plotted over the TCR/pMHC affinity (K_D). Dashed line indicates fold change of 1. Data in (C) are representative of at least $N=3$ independent experiments with different blood donors. Data in (D) is shown as means \pm SDs. Significance of non-zero slope was assessed by an F-test.

61 **CD8 knock-out abolishes therapeutic a3a TCR cross-reactivity to Titin**

62 T cells engineered with the MAGE-A3 specific a3a TCR caused lethal cardiac toxicities in a clinical trial
63 due to cross-reactivity to a lower affinity peptide from the muscle protein Titin (4, 5). Since we have
64 demonstrated that the CD8 co-receptor can decrease T cell ligand discrimination, we decided to investigate
65 whether the cross-reactivity to Titin was CD8 dependent.

66 Given that TCR-T therapies rely on expressing the therapeutic MHC-I restricted TCR in both CD8+
67 cytotoxic and CD4+ helper T cells, we first examined their individual abilities to react to each antigen.
68 Whilst both cytotoxic and helper T cells responded to the on-target MAGE-A3 antigen, only cytotoxic T
69 cells responded to the off-target Titin antigen confirming that cytotoxic T cells are the likely source of
70 autoimmune toxicity (Fig. 2A-B). By knocking out CD8 in cytotoxic cells we abolish activation against
71 Titin without impacting responses to the higher-affinity on-target antigen (Fig. 2C-D). The CD8 KO also
72 abolished the activation of T cells against Nalm6 cells that endogenously express Titin (5) (Fig. 2E).

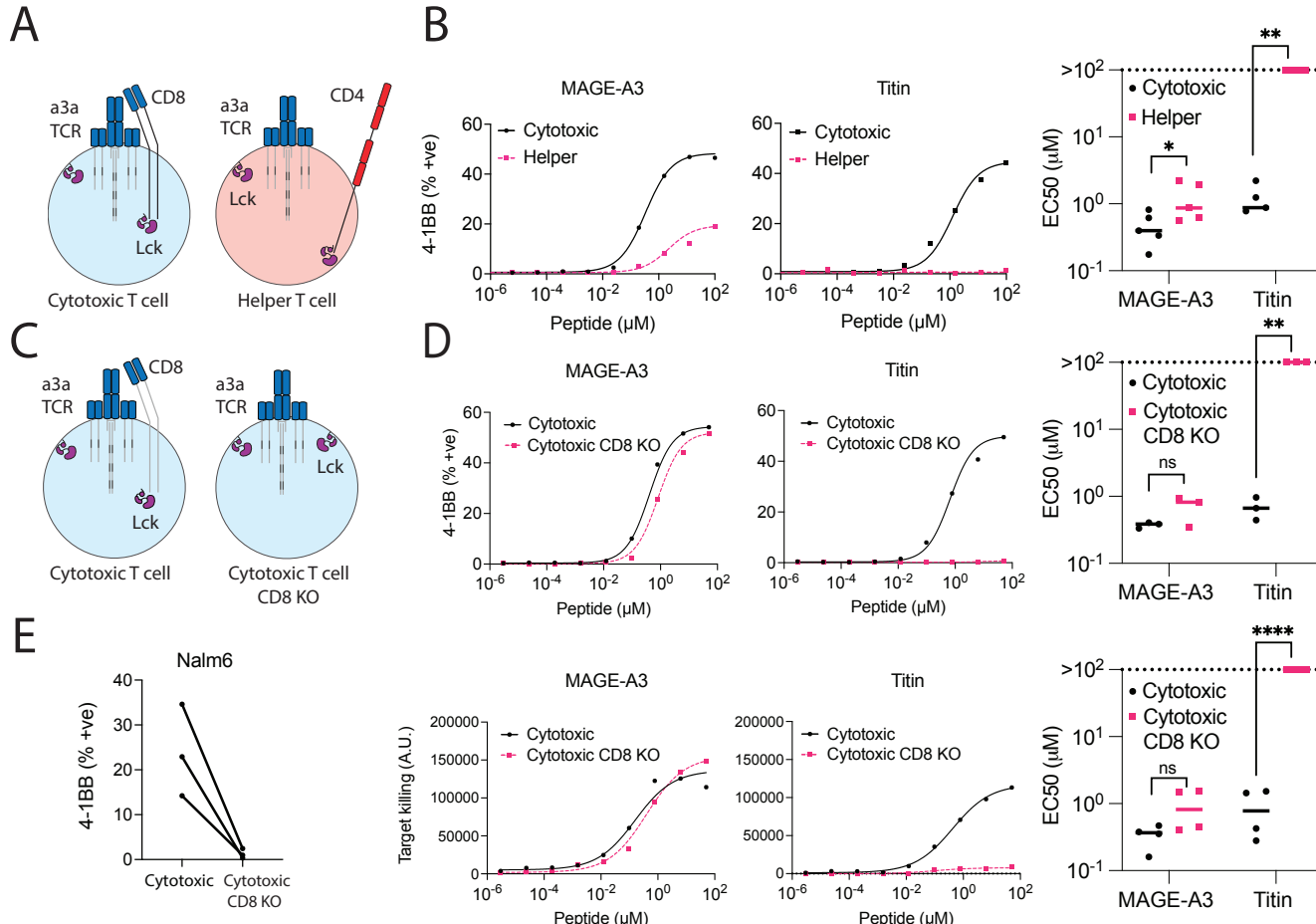


Figure 2: CD8 co-receptor KO abolishes MAGE-A3 TCR cross-reactivity to the self-antigen Titin.

(A) Schematic of helper and cytotoxic T cells transduced with the MAGE-A3 specific a3a TCR. Lck can exist in a free state or a co-receptor bound state. (B) HLA-A1+ T2 cells were titrated with MAGE-A3 or Titin peptides to stimulate cytotoxic or helper a3a TCR-T cells for 20 hours. Representative dose-responses (Left) and mean sensitivity as EC50 (Right). (C) Schematic of WT or CD8 KO cytotoxic a3a TCR-T cells. Lck can exist in a free state or a co-receptor bound state. (D) HLA-A1+ T2 cells were titrated with MAGE-A3 or Titin peptides to stimulate WT or CD8 KO cytotoxic a3a TCR-T cells for 20 hours. Representative dose-responses (Left) and mean sensitivity as EC50 (Right). Data measuring 4-1BB surface activation marker (top) and target cell killing (bottom) are shown. (E) Nalm6 cells endogenously expressing the Titin protein were co-cultured with WT or CD8 KO cytotoxic a3a TCR-T cells for 20 hours. 4-1BB was stained by flow cytometry. Each data point in (E) represents an independent experiment with different blood donors. Each EC50 data point in (B) and (D) represents an independent experiment with different blood donors. P values were determined by paired t-test; ns not significant, *p<0.05, **p<0.01, ***p<0.0001

73 **Helper T cells display enhanced discrimination against pMHC-I antigens due to their incom-
74 patible CD4 co-receptor**

75 The observation that CD4+ helper T cells only responded to the higher-affinity MAGE-A3 antigen whereas
76 CD8+ cytotoxic T cells also responded to the lower-affinity Titin antigen (Fig. 2A-B) suggested that helper
77 T cells may have a different capacity to discriminate ligands.

78 We compared ligand discrimination in helper vs cytotoxic T cells using the NY-ESO-1 c259 TCR plat-
79 form (Fig. 3A). Consistent with the a3a TCR, we found that cytotoxic T cells activated more strongly
80 against low affinity pMHCs than helper T cells (Fig. 3B-C). Interestingly, helper T cells displayed even
81 higher discrimination than CD8 KO cytotoxic T cells (Fig. 3C).

82 The degree to which T cells are able to respond to lower-affinity antigens is partly determined by a
83 kinetic proofreading mechanism that introduces a time-delay between pMHC binding and TCR signalling
84 (22, 29) (Fig. 3D). This time-delay is thought to be determined by biochemical steps that follow pMHC
85 binding, including phosphorylation of ITAMs and ZAP70 by Lck, ZAP70 auto-phosphorylation, and the
86 bridging of ZAP-70 and LAT by Lck (30–32). By fitting the proofreading model directly to the potency
87 over pMHC affinity data (Fig. 3E), we confirmed that the time-delay for helper T cells is even larger than
88 CD8 KO cytotoxic T cells. Thus, high levels of ligand discrimination for helper T cells cannot be explained
89 simply by the absence of CD8 co-receptor alone.

90 Helper T cells express the CD4 co-receptor that like CD8 has an intracellular association with Lck, but
91 unlike CD8 cannot bind the MHC-I antigens targeted by the c259 TCR. We hypothesised that the presence
92 of the incompatible CD4 co-receptor could be responsible for the enhanced discrimination of helper T
93 cells. Indeed, CD4 KO helper T cells displayed improved activation to lower affinity peptides, reducing
94 ligand discrimination compared to wild-type helper T cells (Fig. 3F-I). Therefore, the incompatible CD4
95 co-receptor increases the ligand discrimination of helper T cells targeting pMHC-I antigens.

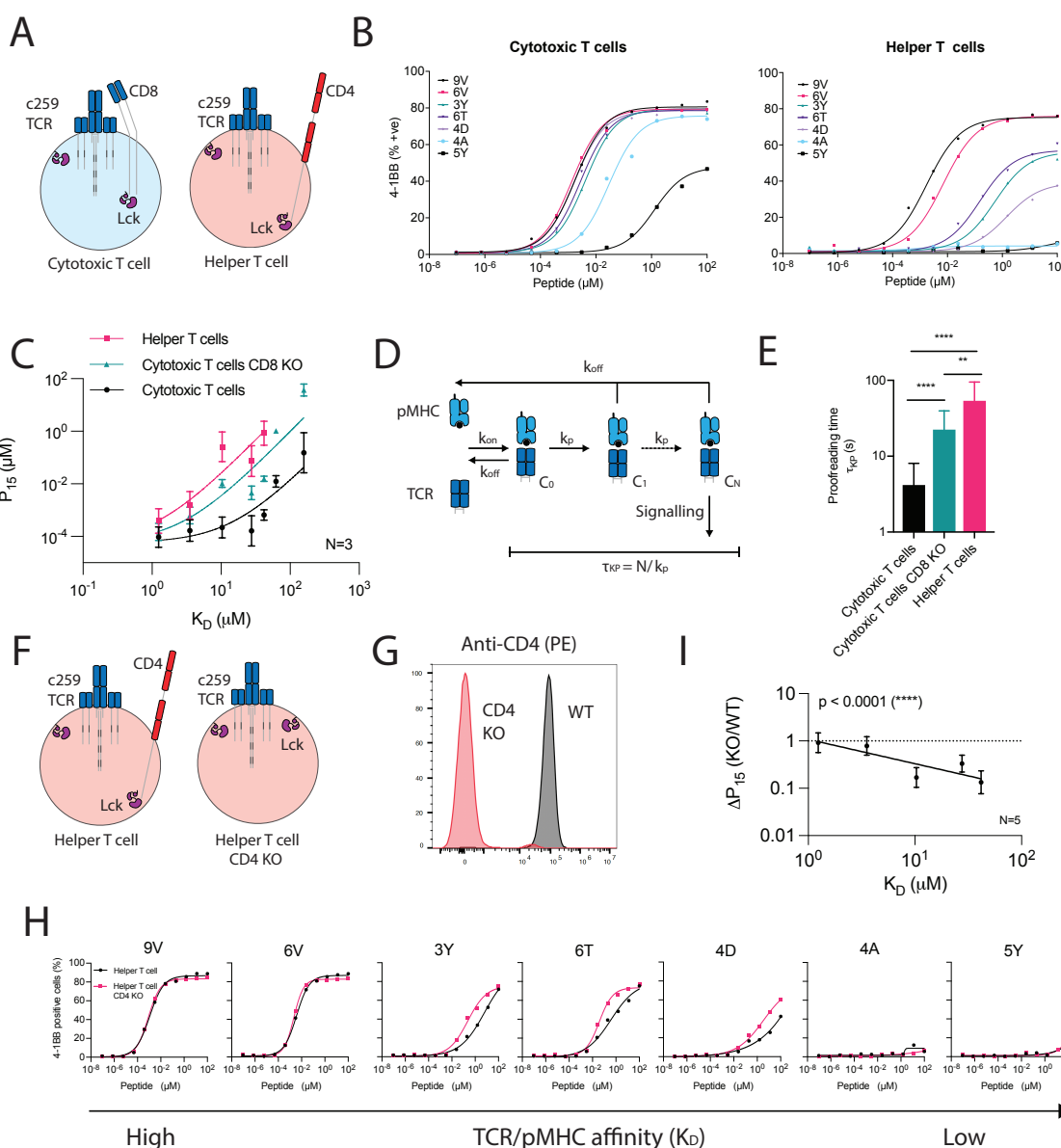


Figure 3: The CD4 co-receptor enhances the discrimination of helper cells expressing an MHC-I restricted TCR. (A) Schematic of helper and cytotoxic T cells transduced with the c259 TCR. (B) Representative ligand discrimination assays using helper and cytotoxic c259 TCR-T cells recognising peptides on U87 target cells. Expression of the 4-1BB activation marker was measured after a 20 hour co-culture. (C) Mean potency (P_{15}) over TCR/pMHC affinity (K_D) from $N=3$ independent blood donors (points) is fitted to the kinetic proofreading model (solid line). (D) Kinetic proofreading introduces a time-delay (τ_{kp}) between pMHC binding (state C_0) and TCR signalling (state C_N) that selectively reduces signalling to low-affinity ligands. (E) Fitted time-delay from the data in panel (C). F-test compares the time-delay between conditions. (F) Schematic of helper WT and CD4 KO c259 TCR-T cells. (G) Flow cytometry staining of CD4 in WT and CD4 KO helper T cells. (H) U87 cells were titrated with each of the 7 NY-ESO-1 peptides to stimulate WT or CD4 KO helper c259 TCR-T cells. 4-1BB expression was measured after 20 hours. (I) Fold change in potency (P_{15}) between CD4 KO and WT helper T cells from (H) is plotted over TCR/pMHC affinity (K_D). Dashed line indicates fold change of 1. Significance of non-zero slope was assessed by an F-test Data in (B), (G) and (H) are representative of at least $N=3$ independent experiments with different blood donors. Data in (I) is shown as means \pm SDs of $N=5$ independent experiments with different blood donors. ns not significant, * $p<0.05$, ** $p<0.01$.

**96 Expression of the incompatible CD4 co-receptor in cytotoxic T cells enhances their ligand
97 discrimination**

98 Since the CD4 co-receptor increased the ability of helper T cells to discriminate ligands using an MHC-I
99 restricted TCR, we examined whether it could also do this in cytotoxic T cells (Fig. 4A). Indeed, expression
100 of CD4 in cytotoxic T cells selectively reduced activation and target killing against lower affinity pMHCs,
101 without affecting responses to the high affinity cognate peptide (Fig. 4B, S6A). Moreover, expression of
102 CD4 in CD8 KO cytotoxic T cells synergised to produce T cells with extremely high levels of discrimi-
103 nation (Fig. 4B-C, S6B-C). For example, whereas wild-type T cells can respond to the lower-affinity 4D
104 peptide, these CD8→CD4 co-receptor switch T cells ignore this same antigen unless its concentration was
105 increased by a dramatic ~3000-fold. Thus, a CD8→CD4 co-receptor switch dramatically increased the
106 ligand discrimination of cytotoxic T cells.

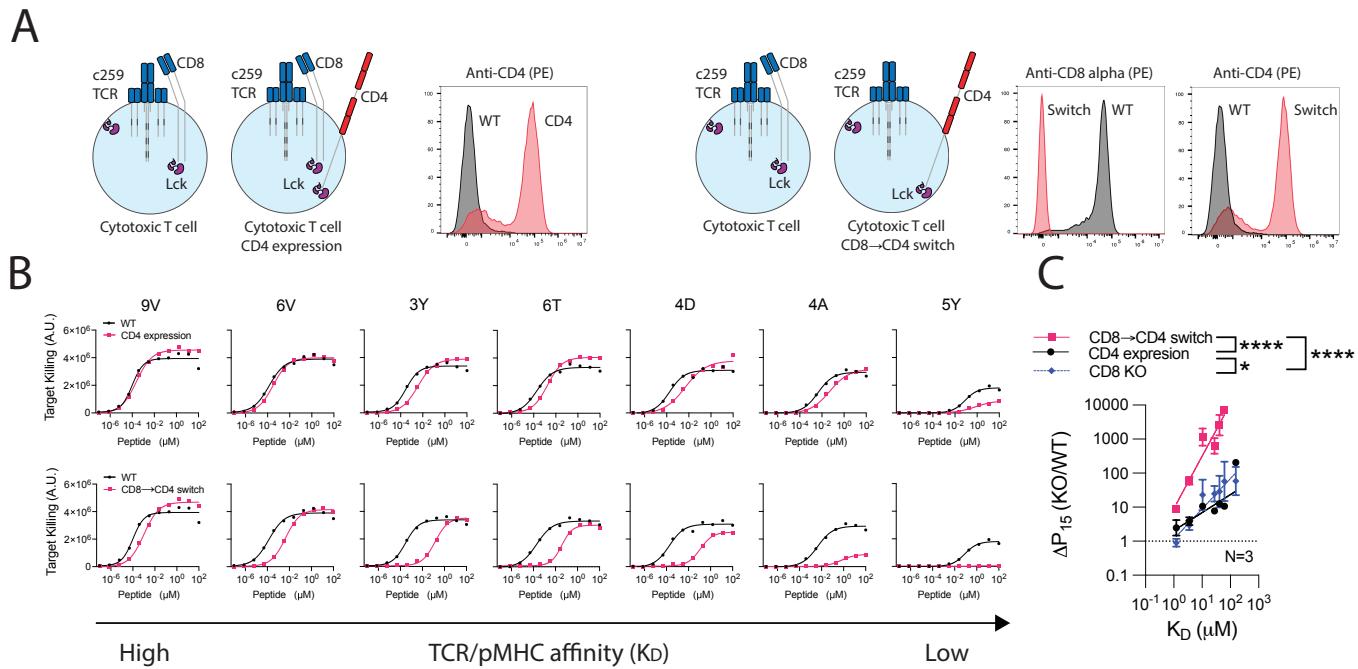


Figure 4: Expression of the incompatible CD4 co-receptor in cytotoxic T cells enhances ligand discrimination. (A) (Left) Schematic of CD4 expression in cytotoxic T cells and flow cytometry staining of CD4 expression. (Right) Schematic of CD8→CD4 co-receptor switch T cells and flow cytometry staining of CD4 and CD8 expression. (B) U87 cells were titrated with each of the 7 NY-ESO-1 peptides to stimulate (Top) WT or CD4 expressing cytotoxic T cells or (Bottom) WT or CD8→CD4 co-receptor switch cytotoxic T cells. Target killing was measured after 20 hours. (C) The fold change in Potency (P15) between the indicated modified and WT cytotoxic T cells over TCR/pMHC affinity (K_D). Data for CD8 KO is shown from Fig 1. Data in (A) and (B) are representative of N=3 independent experiments with different blood donors. Data in (C) is shown as means ± SDs. P values were determined by F-test. *p<0.05, ****p<0.0001.

107 **CD8→CD4 co-receptor switch cytotoxic T cells display reduced cross-reactivity whilst main-**
108 **taining potent target killing**

109 We next used three methods to examine how the increase in ligand discrimination that we report impacts T
110 cell cross-reactivity.

111 In a pooled peptide library that contains a random mixture of peptides, it is expected that the majority
112 of peptides that bind the TCR would do so with low affinity. As a result, we predicted that increasing ligand
113 discrimination would reduce T cell cross-reactivity to a pooled library (Fig. 5A). We stimulated T cells with
114 target cells pulsed with a random pooled 9-mer peptide library, where each position can be any amino acid
115 except cysteine, with a theoretical diversity of 19^9 peptides. Cytotoxic T cells expressing the c259 TCR
116 killed target cells pulsed with the random peptide mixture, but reduced cross-reactive killing was observed
117 in CD8 KO and especially in CD8→CD4 co-receptor switch T cells (Fig. 5B).

118 A positional scanning library includes all single amino acid changes relative to a target peptide (163 NY-
119 ESO-1 variant peptides in the present case). Although cytotoxic c259 TCR-T cells killed targets expressing
120 many of these peptides, CD8 KO cells and CD8→CD4 co-receptor switch T cells display reduced killing to
121 many of these peptides with the exception of the target peptide (Fig. 5C). To confirm that this reduced cross-
122 reactivity was a result of increased ligand discrimination based on affinity, we developed a workflow to use
123 a high-throughput SPR-based instrument to accurately and rapidly measure all 163 TCR/pMHC affinities
124 (Fig. 5D, S7, Table S2). As predicted, the reduced cross-reactivity of CD8 KO and CD8→CD4 co-receptor
125 switch T cells was dependent on affinity with reduced responses observed only to lower-affinity interactions
126 (Fig. 5E-F).

127 Data from positional scanning libraries can also be used to predict TCR off-target cross-reactivities and
128 this method has previously been used to predict potential self peptides recognised by the c259 TCR (8).
129 We found that c259 TCR-T cells responded to a subset of these predicted peptides whose affinity we then
130 measured by SPR (Fig. S8, Table S3). The CD8 KO and especially the CD8→CD4 co-receptor switch
131 T cells displayed reduced responses to target cells presenting these cross-reactive self peptides (Fig. 5G-
132 H, S9). Importantly, this reduced cross-reactivity did not compromise potency to the on-target NY-ESO-1
133 cancer antigen (Fig. 5I). Thus, co-receptor switching can reduce T cell cross-reactivity to increase the safety
134 of TCR-T cell therapies.

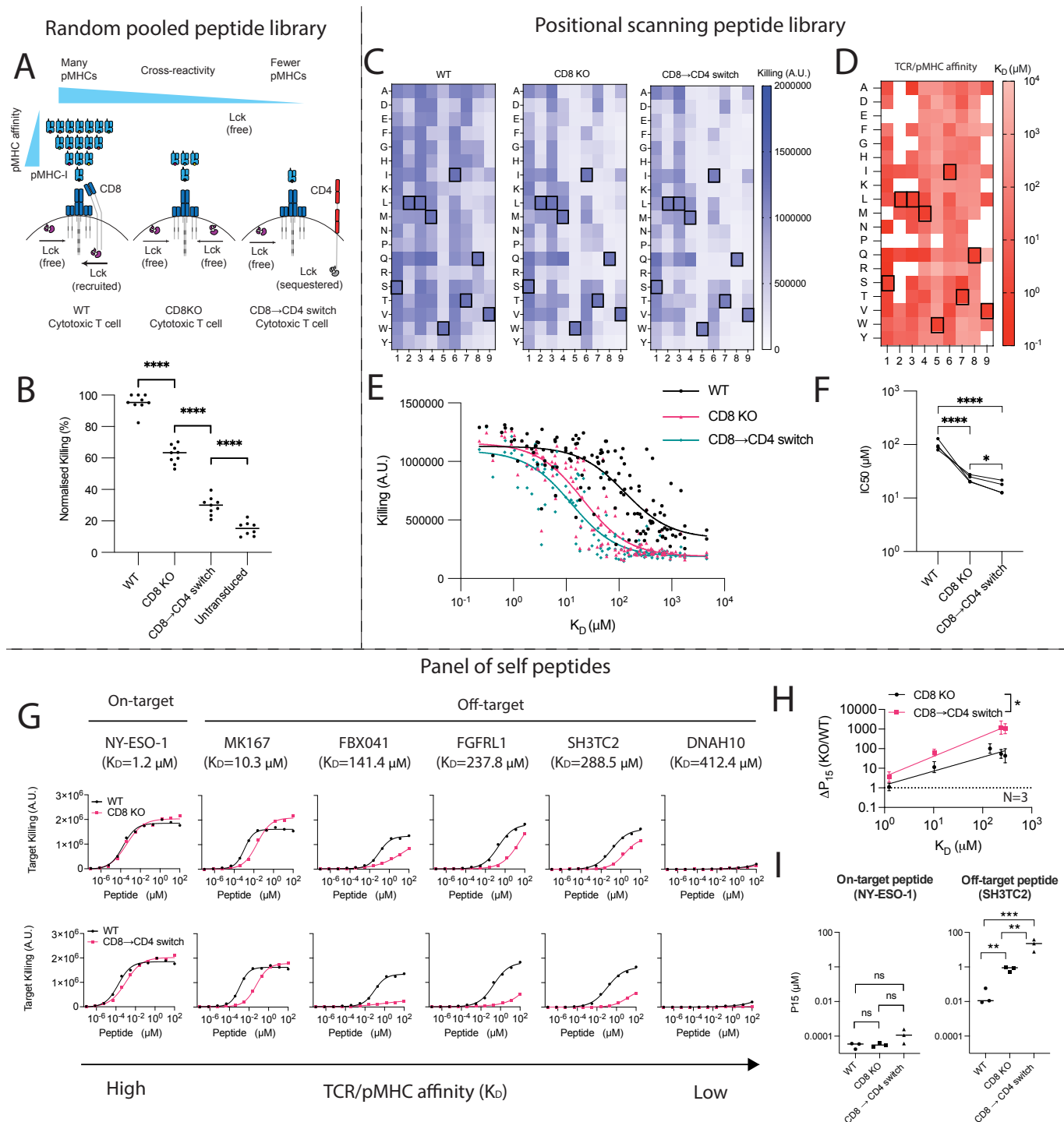


Figure 5: CD8→CD4 co-receptor switch cytotoxic T cells display reduced cross-reactivity to peptide libraries and self peptides without compromising on-target potency.

(A-B) Pooled peptide library. **(A)** Schematic of the predicted cross-reactivity of WT, CD8 KO or CD8→CD4 co-receptor switch cytotoxic T cells. **(B)** U87 cells were loaded with a pooled 9-mer peptide library to stimulate WT, CD8 KO or CD8→CD4 co-receptor switch cytotoxic c259 TCR-T cells. Target killing was measured after 20 hours. Each data point represents a technical replicate from N=3 independent experiments with different blood donors. P values were determined by paired t-test. **(C-F) Positional Scanning Peptide Library.** **(C)** U87 cells were individually loaded with 0.1 μM of each of the 163 peptides in the positional library and co-cultured with T cells. Target killing was measured after 20 hours. Boxed amino acids represent the NY-ESO-1 peptide SLLMWITQV. **(D)** Affinity between c259 TCR and each pMHC in the positional library determined at 37 degrees by a high-throughput SPR method. Mean K_D values are shown from N=3 independent experiments. Boxed amino acids represent the NY-ESO-1 peptide SLLMWITQV. White boxes represent peptides without detectable MHC binding. **(E)** Target cell killing from (C) plotted over the TCR/pMHC K_D from (D). **(F)** IC50 from (E) is plotted with each data point representing an independent experiment with different blood donors. Data in (C) and (E) are representative data from N=4 independent experiments with different blood donors. P values were determined by paired t-test. **(G-I) Predicted self-peptides.** **(G)** U87 cells were titrated with each of the predicted self-peptides to stimulate (Top) WT or CD8 KO cytotoxic c259 TCR-T cells or (Bottom) WT or CD8→CD4 co-receptor switch cytotoxic c259 TCR-T cells. Target killing was measured after 20 hours. **(H)** Fold change in Potency (P15) between modified and WT T cells from (G) is plotted over TCR/pMHC affinity (K_D). Data is shown as means ± SDs. P values were determined by F-test. **(I)** Potency (P15) from (G) is plotted for the indicated peptides. Each data point represents an independent experiment. P values were determined by paired t-test. Data in (G) are representative of N=3 independent experiments with different blood donors. ns not significant, *p<0.05, **p<0.01, ***p<0.001, ****p<0.0001.

135 Discussion

136 It has been estimated that a single T cell can recognise over 10⁶ different peptides (33, 34). This cross-
137 reactivity is an essential feature of adaptive immunity, enabling the limited number of T cell clones within
138 an organism to provide protection against a much larger number of pathogenic peptides. However, T cell
139 cross-reactivity poses a significant challenge to the success of TCR-T therapies as it can lead to lethal
140 off-target toxicities. Identifying safe and effective TCRs remains a critical bottleneck in the development of
141 new therapies. Despite this binding cross-reactivity, T cells use kinetic proofreading to discriminate between
142 high and low affinity peptides (22, 29). Since ligand discrimination emerges not only from TCR binding but
143 from TCR signalling (31, 32), we hypothesised that modifying T cell co-signalling receptors involved in this
144 signalling pathway could be exploited to increase T cell ligand discrimination and reduce cross-reactivity
145 without modifying the TCR. We have demonstrated the ability to increase and decrease ligand discrimination
146 by genetic knockout and/or expression of the surface molecules CD5, CD4, and CD8 in helper/cytotoxic T
147 cells. The CD8→CD4 co-receptor switch produced super selective T cells that display a striking increase in
148 ligand discrimination and reduced cross-reactivity to a pooled and positional scanning libraries, and to self
149 peptides without impacting on-target potency.

150 The CD8 co-receptor plays an essential role in thymic selection but its role in ligand discrimination is
151 debated. Previous work established that CD8 increases T cell activation by stabilising the extracellular TCR-
152 pMHC interaction (35) and by recruiting Lck to the signalling subunits of the TCR-CD3 complex (36). It has
153 been proposed that CD8 can selectively stabilise high-affinity TCR/pMHC interactions through a positive
154 feedback that amplifies differences in binding affinity and hence enhances ligand discrimination (35, 37). On
155 the other hand, it has been suggested that CD8 slows the dissociation rate of TCR/pMHC interactions (38),
156 which preferentially increases the sensitivity to low affinity peptides and hence reduces ligand discrimination

157 (39–41). Our systematic analyses support the latter hypothesis, showing that CD8 KO selectively reduces
158 activation towards lower-affinity antigens and hence CD8 KO increases ligand discrimination.

159 We found that CD4+ helper T cells display higher levels of ligand discrimination compared to CD8+ cy-
160 toxic or CD8 KO cytotoxic T cells recognizing MHC-I antigens. This suggested that the CD4 co-receptor,
161 which binds MHC-II, might further increase ligand discrimination. We confirmed this by showing that CD4
162 KO in helper T cells reduced their ligand discrimination and expression of CD4 in WT or CD8 KO cytotoxic
163 T cells enhanced their ligand discrimination. These findings are consistent with the Lck sequestration model
164 first proposed to understand thymocyte development. This model postulates that CD4/CD8 co-receptors
165 inhibit signalling when they are not able to recognise the ligand recognised by the TCR, by sequestering
166 Lck from the TCR (42–44). We suggest that removal of a compatible co-receptor or the introduction of an
167 incompatible co-receptor increases the proofreading time-delay between pMHC binding and TCR signalling
168 leading to enhanced ligand discrimination (Fig. 3).

169 Whilst increasing the discrimination of therapeutic TCRs can increase their safety, decreasing ligand
170 discrimination has been proposed as an attractive strategy to increase activation against lower affinity im-
171 mune escape peptide variants in tumours with high genomic instability (45). We have identified CD5 KO
172 as a candidate modification to decrease T cell ligand discrimination and our findings are consistent with its
173 negative regulatory function that fine-tunes TCR signalling to maintain T cell tolerance and reduce the risk
174 of autoimmunity (24, 46). Although reducing the function of CD5 has been shown to enhance anti-tumour
175 activity in TCR-T and CAR-T cells (47–49), this may be a double-edge sword because it would also in-
176 crease cross-reactivity and hence the risk of autoimmune toxicities. Similarly, on-going clinical trials have
177 engineered CD4+ helper T cells to express the CD8 co-receptor to increase their potency (50) but our results
178 suggest that this may increase their cross-reactivity and the risk of autoimmune toxicities.

179 Overall, we have demonstrated that super selective T cells with reduced cross-reactivity and enhanced
180 ligand discrimination can be generated without impacting on-target potency and importantly, without mod-
181 ifying the TCR. We have applied the method to the clinical a3a and c259 TCRs showing that it can abolish
182 functional cross-reactivity to self peptides. A limitation of this method is that if a TCR does not bind its
183 target cancer peptide with high affinity, its potency may be reduced by co-receptor switching. Therefore,
184 affinity-maturation might be required for lower-affinity therapeutic TCRs. Given that these super selective
185 T cells are generated by modifying genes extrinsic to the TCR, it has the potential to dramatically increase
186 the safety of TCR-T cell therapies regardless of the therapeutic TCR that is used.

187 **Funding**

188 The work was funded by a Wellcome Trust Senior Fellowship in Basic Biomedical Sciences (207537/Z/17/Z
189 to OD) and by UKRI-Biotechnology and Biological Sciences Research Council (BB/T008784/1 to JCC).

190 **Open access**

191 This research was funded in whole, or in part, by the Wellcome Trust [207537/Z/17/Z]. For the purpose of
192 Open Access, the author has applied a CC BY public copyright licence to any Author Accepted Manuscript
193 version arising from this submission.

194 **Author contributions**

195 Conceptualization (JCC, OD), Data Curation (JCC, AH, MK, AS), Formal Analysis (JCC, AH), Funding
196 Acquisition (OD), Investigation (JCC, AH, MK, AS), Methodology (JCC, VA, AH, MK, AS, PAvDM, OD),
197 Project Administration (OD), Supervision (PAvDM, OD), Visualization (JCC), Writing – Original Draft
198 (JCC, OD), Writing – Review & Editing (JCC, AH, MK, AS, PAvDM, OD)

199 **Materials & Methods**

200 **Cell culture**

201 U87 and HEK cell lines were cultured at 37°C and 10% CO2 in DMEM D6429 media (Sigma-Aldrich)
202 supplemented with 10% FBS, 50 µg/mL Streptomycin and 50 units/mL Penicillin.

203 T2 cells and Nalm6 cells were cultured at 37°C and 10% CO2 in RPMI 1640 (Sigma-Aldrich) supplemented
204 with 10% FBS, 50 µg/mL Streptomycin, 50 units/mL Penicillin.

205 Primary human T cells were isolated from leukocyte cones and cultured at 37°C and 10% CO2 in RPMI
206 1640 (Sigma-Aldrich) supplemented with 10% FBS, 50 µg/mL Streptomycin, 50 units/mL Penicillin and 50
207 U/mL IL2.

208 **Lentivirus production**

209 0.8 Million HEK 293T cells were seeded in a 6-well plate (Day 1) and incubated overnight. Cells in each
210 well were co-transfected (Day 2) using X-tremeGENE™ HP (Roche) with 0.8 µg of the appropriate lentivi-
211 ral transfer plasmid encoding an antigen receptor (1G4 TCR or c259 TCR) and the lentiviral packaging
212 plasmids: pRSV-Rev (0.25 µg), pMDLg/pRRE (0.53 µg), and pVSV-G (0.35 µg). The media was replaced
213 18 hours following transfection (Day 3). 24 hours after the media exchange, the supernatant from one well
214 was harvested, filtered and used for the transduction of 1 Million human T cells (Day 4).

215 **Production of TCR transduced primary human T cells**

216 T cells were isolated from anonymised leukocyte cones (Day 3) purchased from the NHS Blood Donor Cen-
217 tre at the John Radcliffe Hospital (Oxford University Hospitals). As a result of the anonymised nature of the
218 cones, biological sex and gender were not variables in the present study and were therefore randomised, and
219 as a result the authors were blinded to these variables. RosetteSep™ Human CD8+ Enrichment Cocktail
220 (STEMCELL Technologies) was used for cytotoxic T cells or CD4+ T Cell Enrichment Cocktail (STEM-
221 CELL Technologies) for helper T cells. The enrichment cocktail was added at 150 µl/mL of sample and
222 incubated at RT for 20 minutes. The sample was diluted with an equal volume of PBS and layered on
223 Ficoll® Paque Plus (Cytiva) density gradient medium at a 0.8:1 ratio (Ficoll®:Sample).

224 The sample was centrifuged at 1200 g for 30 minutes (brake off). Cells at the interface of the Ficoll® media
225 and plasma were collected (Buffy coat) and washed twice (Centrifuged at 500 g for 5 minutes). Cells were
226 resuspended in complete RPMI media supplemented with IL2 (50 U/mL) at a density of 1 Million cells per
227 mL. Dynabeads® Human T-Activator CD3/CD28 (Thermofisher) were added (1 Million beads per mL) and
228 cells were incubated overnight.

229 1 Million cells were transduced with the filtered lentiviral supernatant (Day 4). On Day 6 and on Day 8, 1
230 mL of media was removed and replaced with 1 mL of fresh medium. On Day 9, Dynabeads® were removed
231 using a magnetic stand (6 days following isolation). Cells were resuspended in fresh media every other day
232 at a density of 1 Million per mL and used for co-culture experiments. 17 days following isolation T cells
233 were discarded.

234 **CRISPR/Cas9 knock-out of T cell proteins**

235 Cas9 ribonucleoproteins (RNPs) were prepared by mixing 8.5 µg of TruCut Cas9 protein v2 (Thermofisher)
236 with 150 pmol of sgRNA mix (TruGuide synthetic grna, Thermofisher) and Opti-MEM (Gibco) to a final
237 volume of 5 µl. The RNPs were incubated for 15 minutes at room temperature.

238 1 Million freshly isolated T cells were washed with Opti-MEM (Gibco) and re-suspended at a density
239 of 20 Million per mL. The T cells were mixed with the RNPs and transferred into a BTX Cuvette Plus
240 electroporation cuvette (2mm gap, Harvard Bioscience). The cells were electroporated using a BTX ECM
241 830 Square Wave Electroporation System (Harvard Bioscience) at 300 V, 2 ms. Immediately following
242 electroporation, the cells were transferred to complete RPMI media supplemented with IL2 and Dynabeads®
243 Human T-Activator CD3/CD28 (Thermofisher) were added.

244 The following sgRNA sequences were used:

245 **CD8 alpha knock-out:**

246 Guide 1: ATACTGTTGTGCGCACATCG
247 Guide 2: GTTAGACGTATCTCGCCGAA
248 Guide 3: GCTGCTGTCCAACCCGACGT
249 Guide 4: GAGCAAGGCGGTCACTGGTA

250

251 **CD5 knock-out:**

252 Guide 1: GCAGACTTTGACGCTTGAC
253 Guide 2: CCGTTCCAACTCGAAGTGCC
254 Guide 3: ATCATCTGCTACGGACAAC
255 Guide 4: AGGTCTACCTCAAGGACGGA

256

257 **CD43 knock-out:**

258 Guide 1: GGCTCGCTAGTAGAGACCAA
259 Guide 2: GCACCAATGGAAGTCCAAAG
260 Guide 3: AGGTTGTTGGCTCAGGTAAA

261

262 **CD2 knock-out:**

263 Guide 1: CAAGGCACCCCAGGTTCCA
264 Guide 2: CAAAGAGATTACGAATGCCT
265 Guide 3: CTTGTAGATATCCTGATCAT
266 Guide 4: GCATCTGAAGACCGATGATC

267

268 **CD11a knock-out (LFA-1):**

269 Guide 1: CTTGGATACCGCGCTCTGC
270 Guide 2: CAAGTACTTGGAGGTATAAGT
271 Guide 3: GTAACACAGGCCACTCAGAT
272 Guide 4: GUAGCUCGAGGCCGGCGCUG

273

274 **CD4 knock-out:**

275 Guide 1: GTCAGCGCGATCATTAGCT
276 Guide 2: GAGGTGCAATTGCTAGTGT
277 Guide 3: AACTGTAAGGCGAGTGGGA
278 Guide 4: CTGTTTCGCTTCAAGGGCC

279

280 **Negative selection of T cell knock-out cells**

281 T cells with residual target protein expression were depleted by antibody staining and bead pull-down. T
282 cells were re-suspended in MACS Buffer (PBS, 0.5% BSA, 2 mM EDTA) at a density of 100 Million
283 cells per mL. Cells were stained with 5 µl of the corresponding PE-labelled antibody per million cells
284 for 15 minutes at 4°C, washed with MACS and re-suspended at a density of 100 Million cells per mL.
285 1 µl of MojoSort anti-PE nanobeads (Biolegend) were added per million cells and incubated on ice for 15
286 minutes. The cells were washed with MACS and the beads were pulled-down magnetically. The supernatant
287 containing the negatively selected cells was collected.

288 **Cellular co-culture assays**

289 50 000 U87 cells in 100 µl of DMEM were seeded per well in a 96-well Flat-bottom plate and incubated
290 overnight. Alternatively, 100 000 T2 cells were placed in each well of a 96-well Flat Bottom plate. Peptides
291 were diluted in DMEM to the appropriate concentration, added to each well containing cells and incubated
292 for 60 minutes at 37°C, 10% CO₂. The media was discarded and 50 000 T cells were added to each well in
293 200 µl of RPMI media. Cells were incubated for 20 hours at 37°C, 5% CO₂. Supernatants were collected for
294 cytotoxicity and ELISA analysis. 25 µl of 100 mM EDTA PBS were added to each well containing the cells
295 and samples were incubated for 5 minutes at 37°C, 5% CO₂. Cells were detached by thoroughly pipetting
296 each well and transferred to a 96-well V-bottom plate.

297 **Flow Cytometry**

298 Cells were stained for 20 minutes at 4°C, washed with PBS and analysed using a BD X-20 flow cytometer
299 or Cytoflex LX Flow cytometer (Beckman Coulter). The starting cell population was gated on a linear
300 SSC-A/FSC-A plot. Single cells were discriminated on a linear FSC-H/FSC-W plot. In co-culture experiments
301 using U87 cells, T cells were gated as CD45 positive. In co-culture experiments using Nalm6 or
302 T2 cells, T cells were gated as CD3 positive. Positive/negative populations were determined with negative
303 controls. Data was analysed using FlowJo v10, RRID:SCR008520 (BD Biosciences) and GraphPad Prism,
304 RRID:SCR002798 (GraphPad Software).

305 **Cytotoxicity assay**

306 Target cell lines were engineered to express the Nluc luciferase (51). A Coelenterazine (CTZ) 2 mM stock
307 solution was prepared in methanol, aliquoted and stored at -80°C. Supernatant from co-culture assays was
308 mixed in a 1:1 ratio with PBS 10 µM CTZ and luminescence was read using a SpectraMax M3 microplate
309 reader (Molecular Devices).

310 **Cytokine ELISA**

311 Invitrogen Human IFN γ ELISA kits (Thermo Fisher Scientific) were used following the manufacturer's
312 protocol to quantify levels of cytokine in diluted T cell supernatant. A SpectraMax M3 microplate reader
313 (Molecular Devices) was used to measure absorbance at 450 nm and 570 nm.

314 **Surface Plasmon Resonance**

315 All SPR experiments were carried out in the Dunn School SPR facility following the methods published
316 on (22). Briefly, c259 TCR/pMHC steady-state binding affinities were measured on a Biacore T200 (GE
317 Healthcare) with a CAP chip using HBS-EP as running buffer. The CAP chip was saturated with streptavidin
318 and biotinylated pMHCs were immobilised to the desired level. A titration of the TCR was flowed through
319 at 37°C. CD58 was immobilised on a reference flow cell at matching levels to those of pMHCs on the
320 remaining flow cells. The signal from the reference flow cell was subtracted (Single referencing) and the

321 average signal from the closest buffer injection was subtracted (Double referencing). Steady-state binding
322 affinity was calculated by fitting the one site-specific binding model ($\text{Response} = \frac{\text{B}_{\max} [\text{TCR}]}{K_D + [\text{TCR}]}$)
323 on GraphPad Prism to double-referenced equilibrium RU values. The B_{\max} was constrained to the inferred
324 B_{\max} from the empirical standard curve, relating maximal antibody binding to maximal TCR binding.

325 **Pooled Peptide Libraries**

326 50 000 U87 cells in 100 μl of DMEM were seeded per well in a 96-well Flat-bottom plate and incubated
327 overnight. The 9-mer pooled peptide library was diluted in DMEM to 100 μM , added to each well containing
328 cells and incubated for 60 minutes at 37°C, 10% CO₂. 50 000 T cells were added to each well in 200 μl
329 of RPMI media. Cells were incubated for 20 hours at 37°C, 5% CO₂. Supernatants were collected for
330 cytotoxicity analysis.

331 **Positional Scanning Peptide Library SPR**

332 To prepare pMHC complexes presenting the local peptide library, a disulfide-stabilized variant of the human
333 MHC-I protein HLA-A*02:01 (DS-A2) was used (52). The DS-A2 protein was produced as described
334 previously (52). Briefly, the DS-A2 and β 2-microglobulin (β 2m) subunits were produced in *E. coli* as
335 inclusion bodies and solubilized in 8 M urea. The protein was then refolded in the presence of GlyLeu,
336 a dipeptide that binds with low affinity to the peptide-binding cleft. The refolded DS-A2– β 2m complexes
337 were purified by size exclusion chromatography on a Superdex S75 10/300 column (GE Healthcare/Cytiva)
338 in HBS-EP buffer (10 mM HEPES pH 7.4, 150 mM NaCl, 3 mM EDTA, and 0.05% Tween 20). Local-
339 library peptides were loaded by incubating the DS-A2– β 2m complex with each peptide for 2 h at room
340 temperature. The pMHC complexes were stored at 4°C until use within 24 h.

341 Soluble c259 TCR was produced as separate TCR α and TCR β chains in *E. coli*. Both chains were
342 recovered as inclusion bodies, solubilised in 100 mM Tris-HCl (pH 8.0), 8 M urea, 2 mM DTT and stored
343 in aliquots at -70°C. For refolding, 30 mg of each TCR chain was added to 1 L of refolding buffer (150 mM
344 Tris-HCl (pH 8.0) 3 M urea, 200 mM Arg-HCl, 0.5 mM EDTA, 0.1 mM PMSF) and stirred for 1 h at 4°C.
345 This was followed by dialysis in 10 L 10 mM Tris-HCl (pH 8.5) buffer for 3 days in total, with the dialysis
346 buffer changed after 1 day. The refolded c259 TCR was purified using anion exchange chromatography
347 (HiTrap Q HP; Cytiva), followed by size exclusion chromatography (Superdex 200 Increase; Cytiva) in
348 HBS-EP Buffer. Purified c259 was used within 48 h.

349 High-throughput affinity measurements of c259 TCR binding to MHC loaded with the peptide library
350 were performed using LSA or LSA^{XT} (Carterra). Each pMHC was immobilised via biotin-streptavidin
351 binding on a different spot of the SAHC30M biosensor (Carterra) for 20 min, resulting in immobilisation
352 levels between 200 and 900 RUs. Measurements were performed in HBS-EP Buffer at 37 °C. A 2-fold
353 dilution series of c259 TCR was prepared in HBS-EP buffer, with the highest concentration between 100 -
354 130 μM . Starting with the highest dilution, increasing concentrations of c259 were injected over the chip for
355 5 min, followed by 5 -10 min of dissociation, without regeneration. Afterwards, a β 2m specific antibody
356 (clone B2M-01 (Thermo Fisher Scientific) or BBM.1 (Absolute Antibody)) was injected for 10 min. The
357 resulting data was analysed using Kinetics Software (Carterra). Any spikes were removed from the data,
358 before referencing against empty control spots or spots immobilised with CD86 at matching immobilisation
359 levels. The final in a series 6 buffer injection before TCR injection was subtracted from the data for double

360 referencing. Subsequently, the steady state binding RU was calculated by taking the average RU from over
361 20 seconds. Steady-state analysis was performed to obtain the K_D values. First, steady-state data was
362 fitted with a one site-specific binding model ($\text{Response} = B_{\max} [\text{TCR}] / (K_D + [\text{TCR}])$), with K_D and B_{\max}
363 unconstrained. We then constructed an empirical standard curve using high affinity pMHCs ($K_D < 20\mu\text{M}$)
364 to relate maximal anti- β 2m binding to TCR B_{\max} . Next, steady state data for all pMHCs were fitted with
365 a one site-specific binding model with B_{\max} constrained to the B_{\max} inferred from the empirical standard
366 curve. We excluded K_D values for peptides, where we observed little or no anti- β 2m binding responses,
367 indicating that the pMHC complex was unstable and lost the peptide over time (indicated as N/A in Table
368 2). We further excluded K_D values for pMHC that produced a TCR binding response of less than 5 RU
369 (indicated as non-binders (NB) in Table 2).

370 **Data analysis**

371 EC_{50} is calculated as the concentration of antigen required to elicit 50% of the maximum response deter-
372 mined for each condition individually whereas P_{15} is calculated as the concentration of antigen required to
373 elicit 15% of the maximum activation.

374 The study is largely focused on comparing antigen sensitivity using EC_{50} or P_{15} measures, which we
375 have found displays standard deviations of 0.2 (on log-transformed values). The smallest effective size
376 that we aimed to resolve was 3-fold changes (a difference of 0.47 on log-transformed values) and a power
377 calculation shows that this can be resolved with a power of 80% (alpha at 0.05) using three samples in
378 each group. Therefore, all experiments relied on a minimum of 3 independent donors.

379 **Data Availability**

380 This study includes no data deposited in external repositories.

381 **Disclosure and competing interests statement**

382 JCC, PAvdM, and OD have financial interests in a filed patent application related to this technology.

383 **Acknowledgements**

384 We thank Malcolm Sim, Yardena Samuels, Shira Sagie-Groher, and Tomer Babu for helpful discussions.
385 We thank Jonathan Popplewell for assisting with the LSA SPR experiments and Carterra Ltd for providing
386 sensor chips.

387 **Ethics**

388 Human research participants: Ethical approval was provided by the Medical Sciences Inter-divisional Re-
389 search Ethics Committee (IDREC) at the University of Oxford (R51997/RE001).

390 References

- 391 1. Baulu E, Gardet C, Chuvin N, Depil S (2023) TCR-engineered T cell therapy in solid tumors: State of
392 the art and perspectives. *Science Advances* 9.
- 393 2. Peri A, et al. (2023) The landscape of T cell antigens for cancer immunotherapy. *Nature Cancer* 2023
394 4:7 4:937–954.
- 395 3. Morgan RA, et al. (2014) Cancer regression and neurologic toxicity following anti-mage- a3 tcr gene
396 therapy richard. *J Immunother*. 36:133–151.
- 397 4. Linette GP, et al. (2013) Cardiovascular toxicity and titin cross-reactivity of affinity-enhanced t cells in
398 myeloma and melanoma. *Blood* 122:863–871.
- 399 5. Cameron BJ, et al. (2013) Identification of a titin-derived hla-a1-presented peptide as a cross-reactive
400 target for engineered mage a3-directed t cells. *Science Translational Medicine* 5.
- 401 6. Shafer P, Kelly LM, Hoyos V (2022) Cancer Therapy With TCR-Engineered T Cells: Current Strate-
402 gies, Challenges, and Prospects. *Frontiers in Immunology* 13:835762.
- 403 7. Malviya M, et al. (2023) Challenges and solutions for therapeutic TCR-based agents. *Immunological
404 Reviews* 320:58–82.
- 405 8. Karapetyan AR, et al. (2019) TCR fingerprinting and off-target peptide identification. *Frontiers in
406 Immunology* 10.
- 407 9. Kula T, et al. (2019) T-Scan: A Genome-wide Method for the Systematic Discovery of T Cell Epitopes.
408 *Cell* 178.
- 409 10. Dobson CS, et al. (2022) Antigen identification and high-throughput interaction mapping by repro-
410 gramming viral entry. *Nature Methods* 19.
- 411 11. Genolet R, et al. (2023) TCR sequencing and cloning methods for repertoire analysis and isolation of
412 tumor-reactive TCRs. *Cell Reports Methods* 3.
- 413 12. Ishii K, et al. (2023) Multi-tiered approach to detect autoimmune cross-reactivity of therapeutic T cell
414 receptors. *Science Advances* 9.
- 415 13. Foldvari Z, et al. (2023) A systematic safety pipeline for selection of T-cell receptors to enter clinical
416 use. *npj Vaccines* 8.
- 417 14. Drost F, et al. (2024) Predicting T cell receptor functionality against mutant epitopes. *Cell Genomics*
418 0:100634.
- 419 15. Pétremand R, et al. (2024) Identification of clinically relevant T cell receptors for personalized T cell
420 therapy using combinatorial algorithms. *Nature Biotechnology*.
- 421 16. Vazquez-Lombardi R, et al. (2022) High-throughput T cell receptor engineering by functional screening
422 identifies candidates with enhanced potency and specificity. *Immunity* 55:1953–1966.
- 423 17. Hellman LM, et al. (2019) Improving T Cell Receptor On-Target Specificity via Structure-Guided
424 Design. *Molecular Therapy* 27:300–313.

- 425 18. Rosenberg AM, Ayres CM, Medina-Cucurella AV, Whitehead TA, Baker BM (2024) Enhanced T cell
426 receptor specificity through framework engineering. *Frontiers in Immunology* 15.
- 427 19. Zhao X, et al. (2022) Tuning t cell receptor sensitivity through catch bond engineering. *Science* 376.
- 428 20. Chen L, Flies DB (2013) Molecular mechanisms of t cell co-stimulation and co-inhibition. *Nature
429 Reviews Immunology* 13:227–242.
- 430 21. Gyurdieva A, et al. (2022) Biomarker correlates with response to NY-ESO-1 TCR T cells in patients
431 with synovial sarcoma. *Nature Communications* 13.
- 432 22. Pettmann J, et al. (2021) The discriminatory power of the t cell receptor. *eLife* 10:1–42.
- 433 23. Wooldridge L, et al. (2012) A single autoimmune t cell receptor recognizes more than a million different
434 peptides. *Journal of Biological Chemistry* 287:1168–1177.
- 435 24. Azzam HS, et al. (2001) Fine Tuning of TCR Signaling by CD5. *The Journal of Immunology* 166:5464–
436 5472.
- 437 25. Allard JF, Dushek O, Coombs D, van der Merwe PA (2012) Mechanical modulation of receptor-ligand
438 interactions at cell-cell interfaces. *Biophysical Journal* 102:1265–1273.
- 439 26. Pettmann J, et al. (2023) Mechanical forces impair antigen discrimination by reducing differences in
440 T-cell receptor/peptide–MHC off-rates. *The EMBO Journal* 42.
- 441 27. Robbins PF, et al. (2008) Single and Dual Amino Acid Substitutions in TCR CDRs Can Enhance
442 Antigen-Specific T Cell Functions. *The Journal of Immunology* 180:6116–6131.
- 443 28. Chen JL, et al. (2005) Structural and kinetic basis for heightened immunogenicity of t cell vaccines.
444 *The Journal of experimental medicine* 201:1243–55.
- 445 29. McKeithan TW (1995) Kinetic proofreading in t-cell receptor signal transduction. *Proceedings of the
446 National Academy of Sciences of the United States of America* 92:5042–6.
- 447 30. Lo WL, et al. (2018) Lck promotes Zap70-dependent LAT phosphorylation by bridging Zap70 to LAT.
448 *Nature Immunology* 19:733–741.
- 449 31. Goyette J, et al. (2022) Dephosphorylation accelerates the dissociation of ZAP70 from the T cell
450 receptor. *Proceedings of the National Academy of Sciences* 119.
- 451 32. McAfee DB, et al. (2022) Discrete LAT condensates encode antigen information from single
452 pMHC:TCR binding events. *Nature Communications* 13.
- 453 33. Mason D (1998) A very high level of crossreactivity is an essential feature of the T-cell receptor.
454 *Immunology Today* 19:395–404.
- 455 34. Wooldridge L, et al. (2012) A single autoimmune T cell receptor recognizes more than a million
456 different peptides. *Journal of Biological Chemistry* 287:1168–1177.
- 457 35. Jiang N, et al. (2011) Two-Stage Cooperative T Cell Receptor-Peptide Major Histocompatibility
458 Complex-CD8 Trimolecular Interactions Amplify Antigen Discrimination. *Immunity* 34:13–23.
- 459 36. Veillette A, Bookman MA, Horak EM, Bolen JB (1988) The CD4 and CD8 T cell surface antigens are
460 associated with the internal membrane tyrosine-protein kinase p56lck. *Cell* 55:301–308.

- 461 37. Hong J, et al. (2018) A tcr mechanotransduction signaling loop induces negative selection in the thymus.
462 *Nature Immunology* 19:1379–1390.
- 463 38. Wooldridge L, et al. (2005) Interaction between the CD8 coreceptor and major histocompatibility
464 complex class I stabilizes T cell receptor-antigen complexes at the cell surface. *Journal of Biological
465 Chemistry* 280:27491–27501.
- 466 39. Wooldridge L, et al. (2010) Cd8 controls t cell cross-reactivity. *The Journal of Immunology* 185:4625–
467 4632.
- 468 40. Clement M, et al. (2016) Targeted suppression of autoreactive CD8+ T-cell activation using blocking
469 anti-CD8 antibodies. *Scientific Reports* 6.
- 470 41. Laugel B, et al. (2007) Different t cell receptor affinity thresholds and cd8 coreceptor dependence govern
471 cytotoxic t lymphocyte activation and tetramer binding properties. *Journal of Biological Chemistry*
472 282:23799–23810.
- 473 42. Van Laethem F, et al. (2007) Deletion of CD4 and CD8 Coreceptors Permits Generation of $\alpha\beta$ T Cells
474 that Recognize Antigens Independently of the MHC. *Immunity* 27:735–750.
- 475 43. Chervin AS, Stone JD, Bowerman NA, Kranz DM (2009) Cutting Edge: Inhibitory Effects of CD4 and
476 CD8 on T Cell Activation Induced by High-Affinity Noncognate Ligands. *The Journal of Immunology*
477 183:7639–7643.
- 478 44. Van Laethem F, et al. (2013) XLck availability during thymic selection determines the recognition
479 specificity of the T cell repertoire. *Cell* 154:1326.
- 480 45. Spear TT, et al. (2016) Hepatitis C virus-cross-reactive TCR gene-modified T cells: a model for im-
481 munotherapy against diseases with genomic instability. *Journal of Leukocyte Biology* 100:545–557.
- 482 46. Hawiger D, Masilamani RF, Bettelli E, Kuchroo VK, Nussenzweig MC (2004) Immunological Unre-
483 sponsiveness Characterized by Increased Expression of CD5 on Peripheral T Cells Induced by Dendritic
484 Cells In Vivo. *Immunity* 20:695–705.
- 485 47. Matson CA, et al. (2020) CD5 dynamically calibrates basal NF- κ B signaling in T cells during thymic
486 development and peripheral activation. *Proceedings of the National Academy of Sciences* 117:14342–
487 14353.
- 488 48. Chun I, et al. (2020) CRISPR-Cas9 Knock out of CD5 Enhances the Anti-Tumor Activity of Chimeric
489 Antigen Receptor T Cells. *Blood* 136:51–52.
- 490 49. Patel RP, et al. (2024) CD5 deletion enhances the antitumor activity of adoptive T cell therapies. *Science
491 Immunology* 9:6509.
- 492 50. Anderson VE, et al. (2023) Enhancing Efficacy of TCR-engineered CD4+ T Cells Via Coexpression of
493 CD8 α . *Journal of Immunotherapy* 46:132–144.
- 494 51. Matta H, et al. (2018) Development and characterization of a novel luciferase based cytotoxicity assay.
495 *Scientific Reports* 8.
- 496 52. Saini SK, et al. (2019) Empty peptide-receptive MHC class I molecules for efficient detection of
497 antigen-specific T cells. *Science Immunology* 4:9039.

498 **Supplementary Figures**

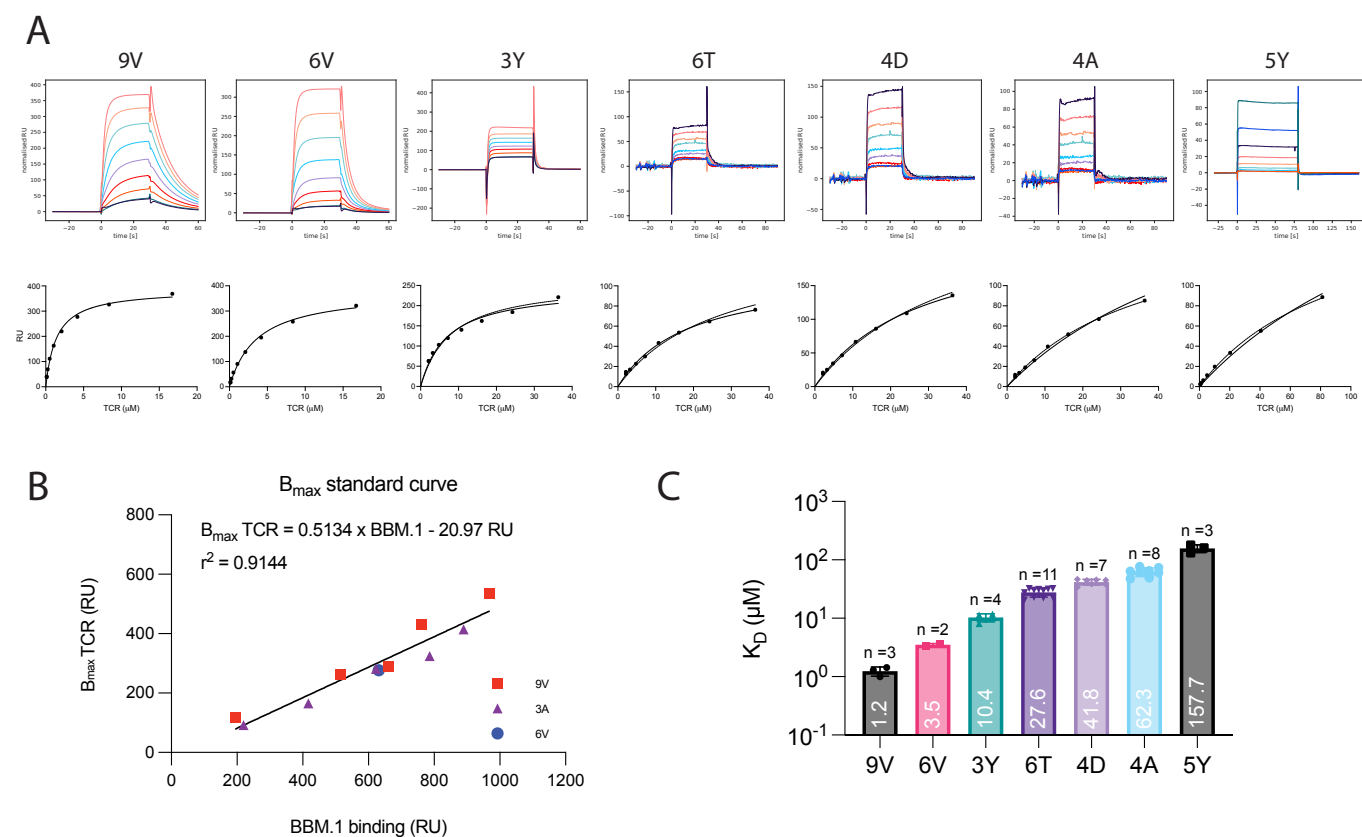
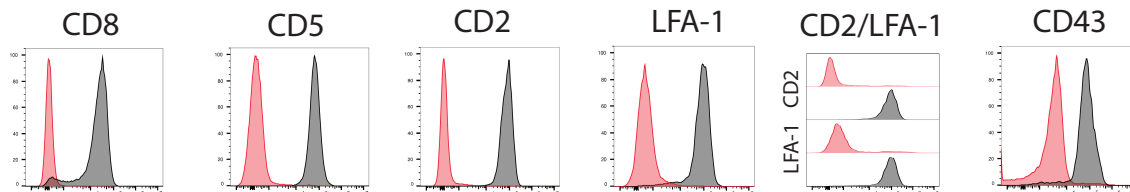


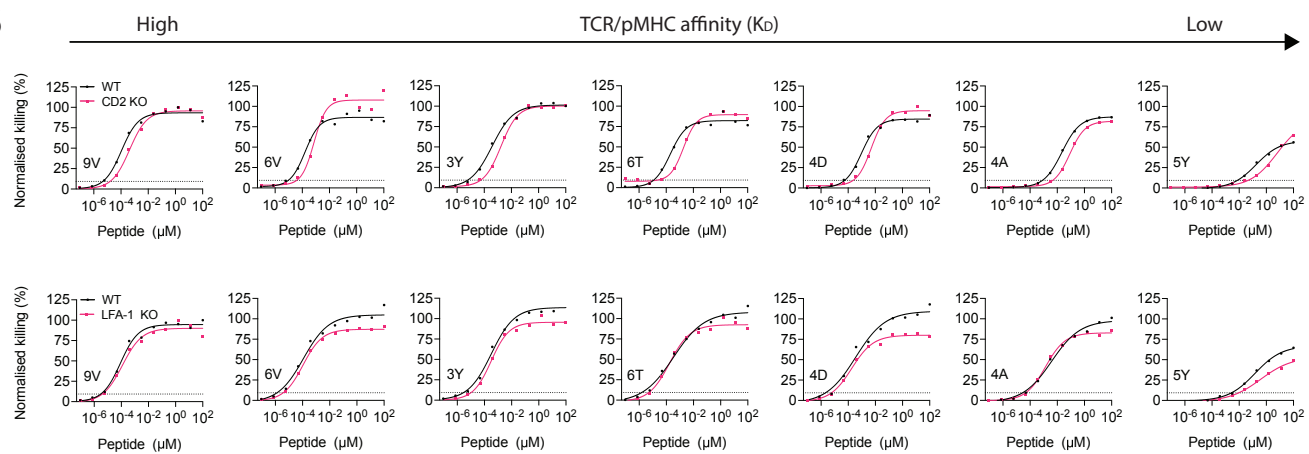
Figure S1: Establishing a panel of peptides that bind the c259 TCR with a range of affinities as measured by SPR at 37°C.

(A) (Top) Representative SPR sensograms depicting injections of increasing concentrations of the c259 TCR. (Bottom) Representative steady-state curves of c259 TCR binding to different pMHCs. K_D was calculated by constraining B_{\max} (dashed line) or fitting B_{\max} (solid line). (B) Empirical standard curve relating the binding of the BBM.1 antibody (x-axis) to the fitted TCR B_{\max} . Only data for the higher-affinity pMHCs is used to generate the standard curve. (C) Steady-state binding affinity for the selected 7-peptide panel. Barplot represents mean $K_D \pm \text{SDs}$. The affinities were calculated by constraining B_{\max} to the value obtained from the standard curve in (B) based on the amount of BBM.1 antibody that bound the chip surface (see Methods for details). All data fitting was performed using a one site-specific binding model in GraphPad Prism.

A



B



C

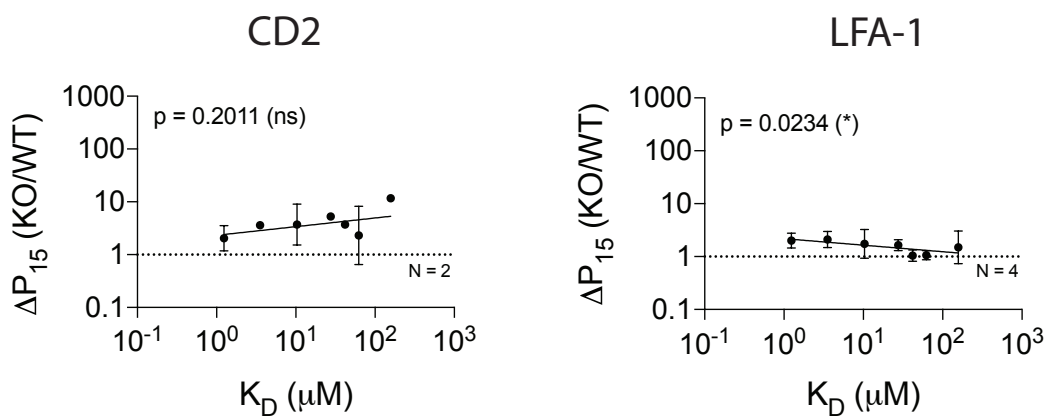


Figure S2: The impact of different T cell co-signalling receptors on ligand sensitivity and discrimination using target cell killing. (A) Flow cytometry staining of WT cells (Black) or KO T cells (Red). (B) U87 cells were titrated with each of the 7 NY-ESO-1 peptides to stimulate WT or KO c259 TCR-T cells. Killing of the target U87 cells was measured after 20 hours. Dashed line indicates potency (P15). (C) Change in potency over affinity as described in Fig. 1D. Data in (A) and (B) are representative of at least N=2 independent experiments with different blood donors. Dashed line in (C) indicates fold change of 1. Data in (C) is shown as means \pm SDs. Significance of non-zero slope was assessed by an F-test.

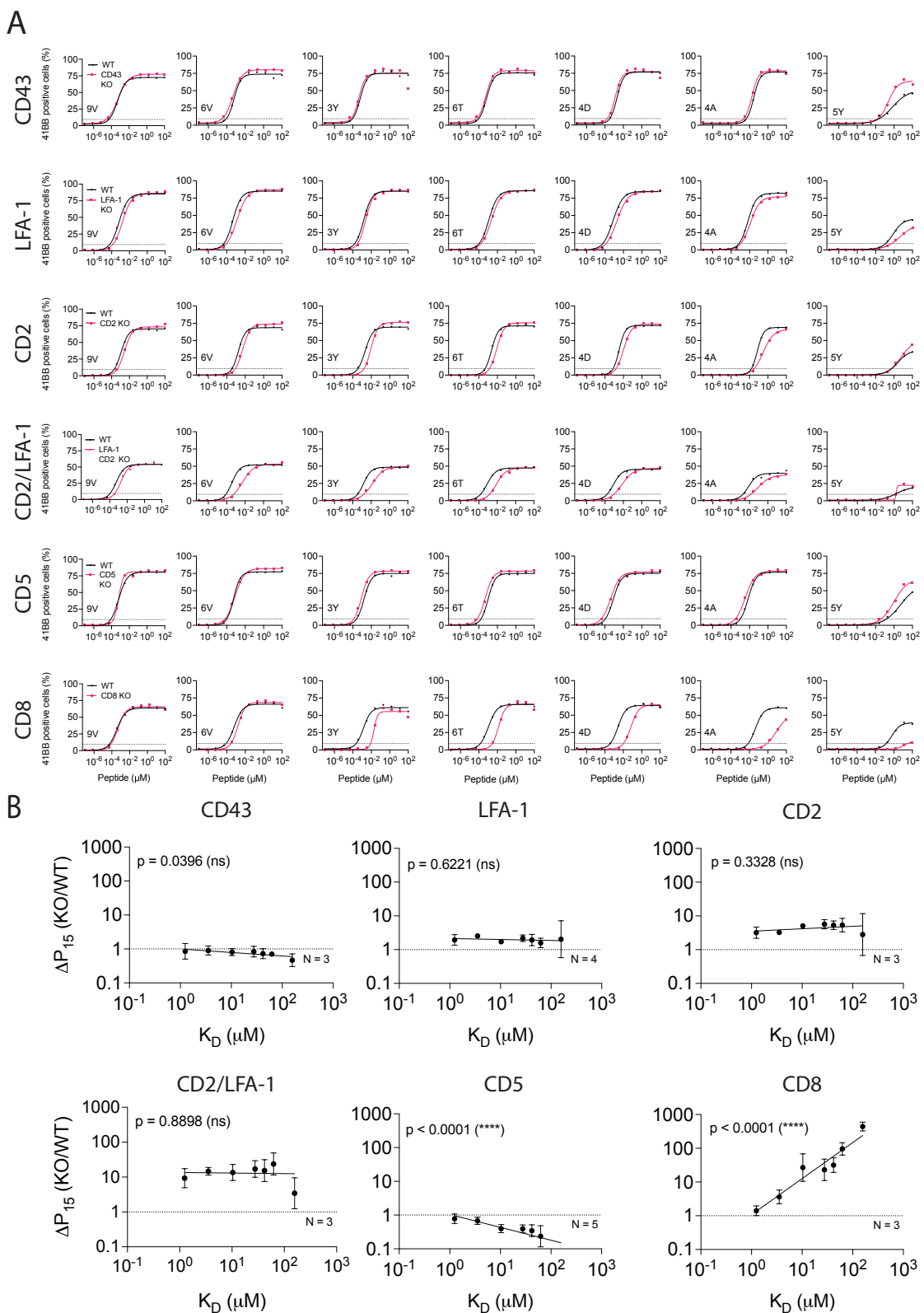


Figure S3: The impact of different T cell co-signalling receptors on ligand sensitivity and discrimination using 4-1BB activation marker. (A) Representative dose-response and (B) Change in potency over affinity as described in Fig. 1D for target killing. Data in (A) are representative of at least N=3 independent experiments with different blood donors. Dashed line in (B) indicates fold change of 1. Data is shown as means \pm SDs. Significance of non-zero slope was assessed by an F-test.

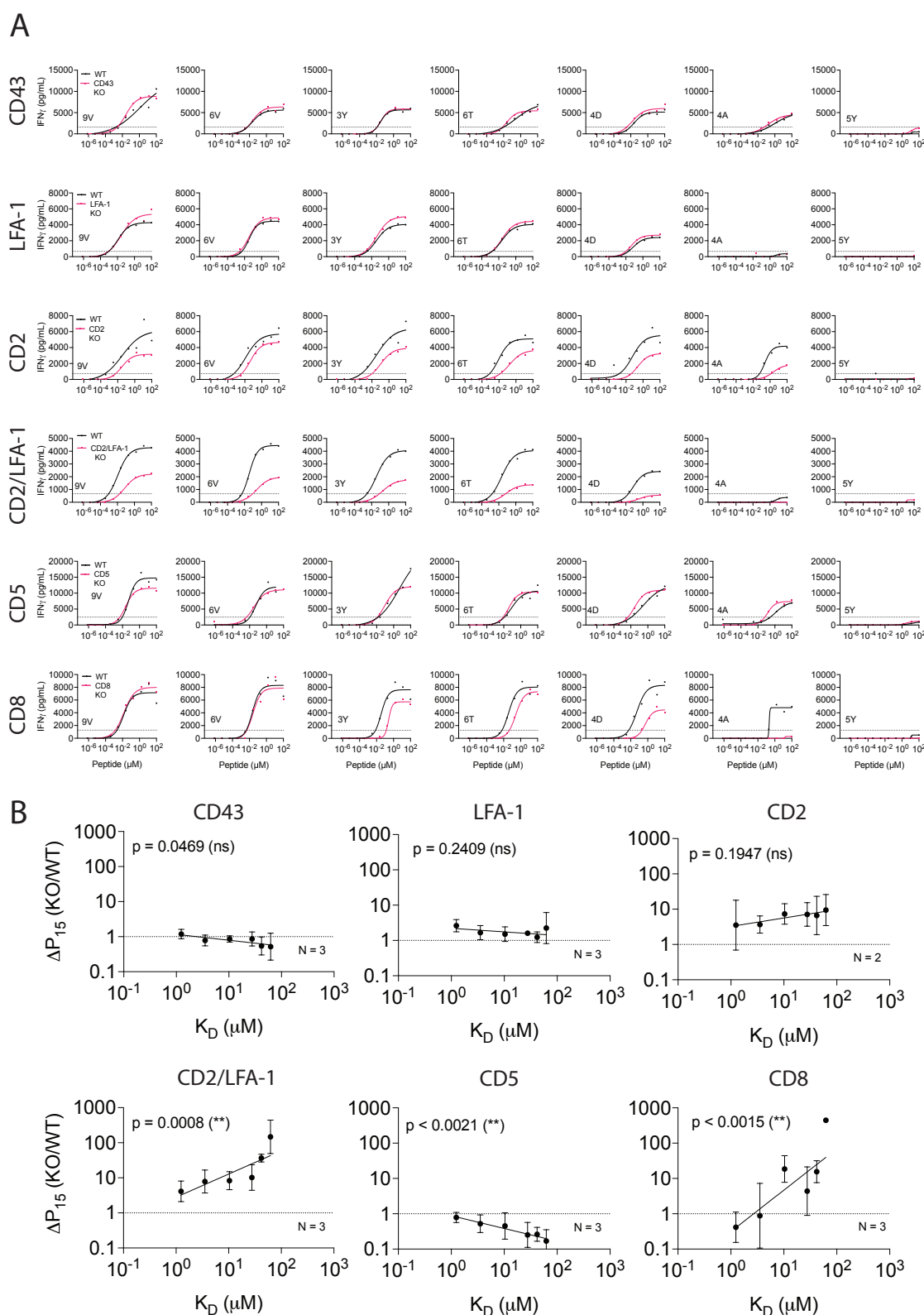


Figure S4: The impact of different T cell co-signalling receptors on ligand sensitivity and discrimination using the secreted cytokine IFN γ . (A) Representative dose-response and (B) Change in potency over affinity as described in Fig. 1D for target killing. Data in (A) are representative of at least $N=2$ independent experiments with different blood donors. Dashed line in (B) indicates fold change of 1. Data is shown as means \pm SDs. Significance of non-zero slope was assessed by an F-test.

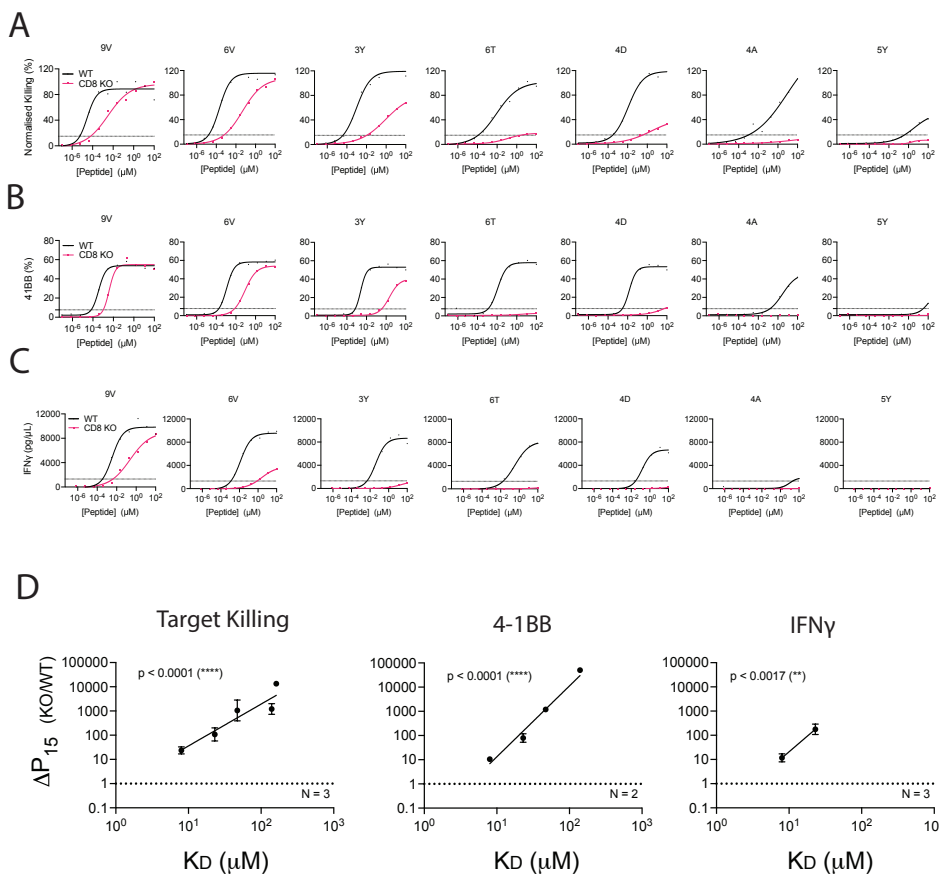


Figure S5: CD8 KO increases the ligand discrimination of the 1G4 TCR.

(A to C) U87 cells were titrated with each of the 7 NY-ESO-1 peptides to stimulate WT or KO 1G4 TCR-T cells. (A) 4-1BB expression was measured after 20 hours. (B) Killing of the target U87 cells was measured after 20 hours. (C) IFN γ secretion was measured after 20 hours. (D) Fold change in potency (P15) between KO and WT T cells plotted over TCR/pMHC affinity (K_D) (22). Dashed line indicates fold change of 1. Data is shown as means \pm SDs. Data in (A), (B) and (C) are representative of at least N=2 independent experiments with different blood donors. Significance of non-zero slope was assessed by an F-test.

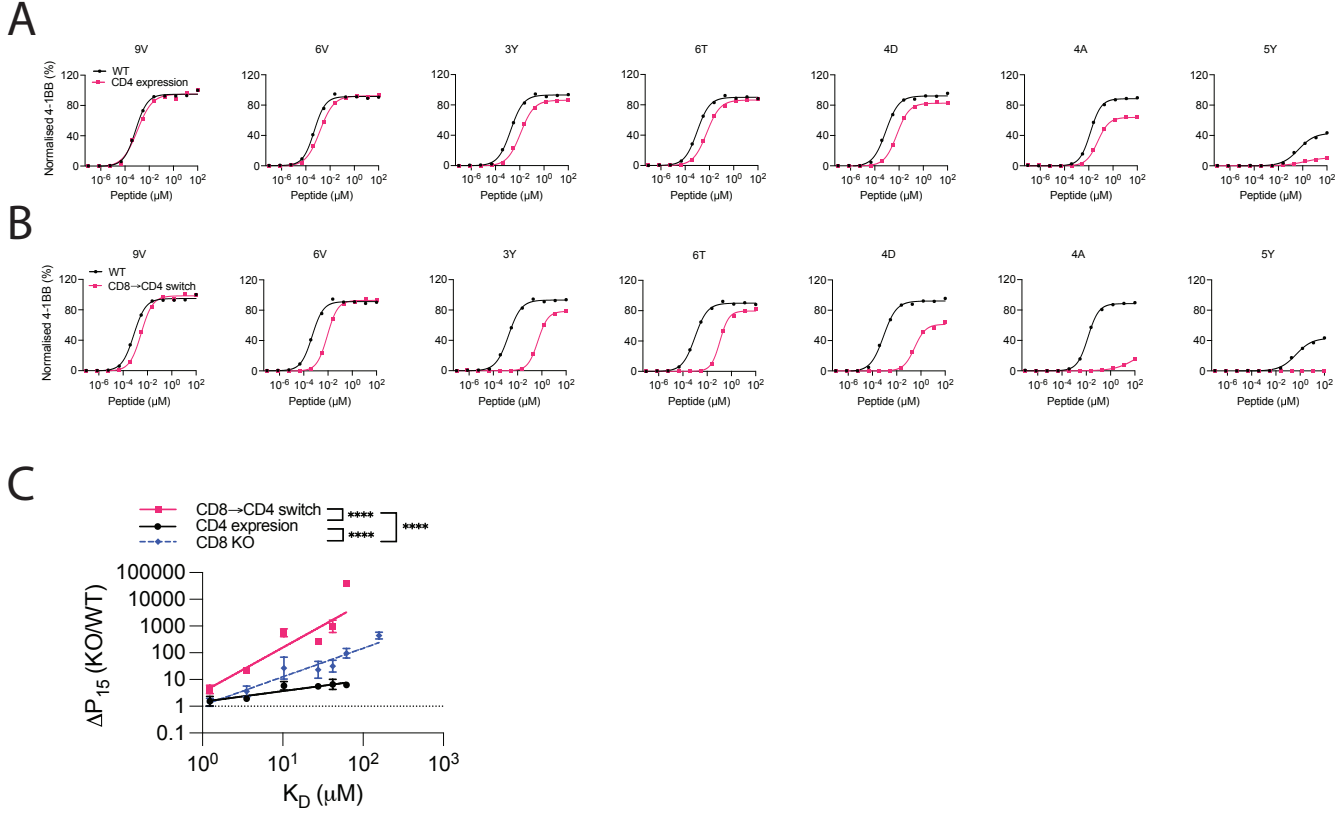


Figure S6: Expression of the incompatible CD4 co-receptor in cytotoxic T cells enhances ligand discrimination (4-1BB).

(A) U87 cells were titrated with each of the 7 NY-ESO-1 peptides to stimulate WT or CD4 expressing cytotoxic c259 TCR-T cells. 4-1BB expression was measured after 20 hours. (B) U87 cells were titrated with each of the 7 NY-ESO-1 peptides to stimulate WT or CD8 \rightarrow CD4 co-receptor switch cytotoxic c259 TCR-T cells. 4-1BB expression was measured after 20 hours. (C) Fold change in potency (P15) between modified and WT T cells from (A,B) is plotted over TCR/pMHC affinity (K_D). Data for CD8 KO is shown from Fig S3. Data is shown as means \pm SDs. Data in (A) and (B) are representative of N=3 independent experiments with different blood donors. P value was determined by an F-test. ****p<0.0001.

A

Workflow for parallel measurements
of 163 TCR/pMHC affinities
using SPR

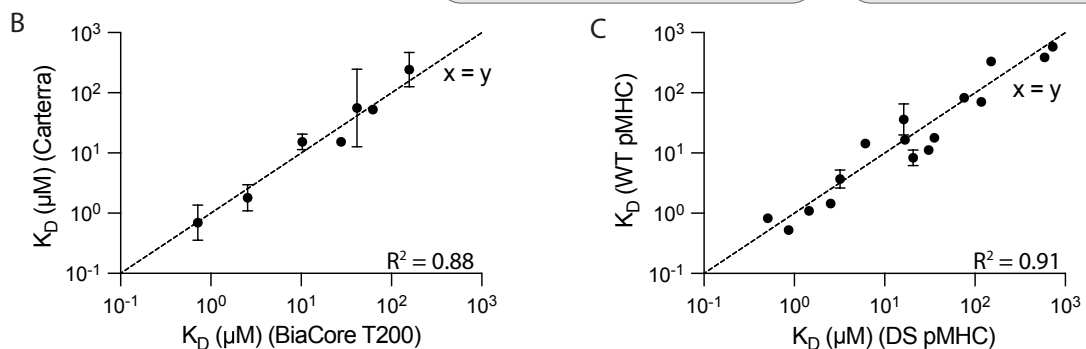
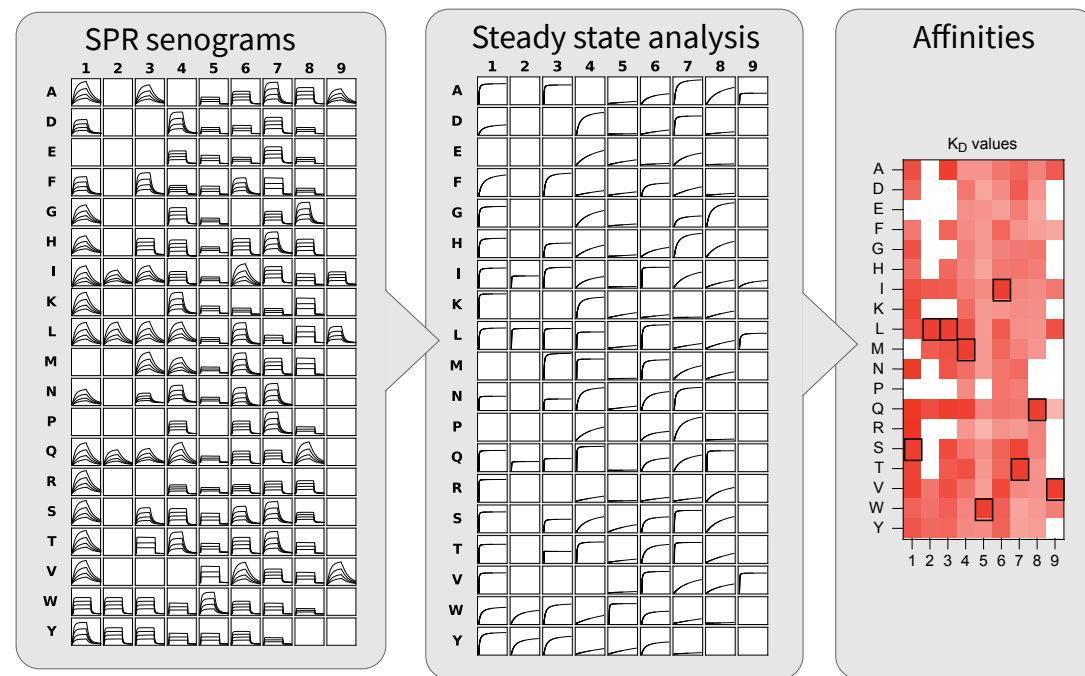
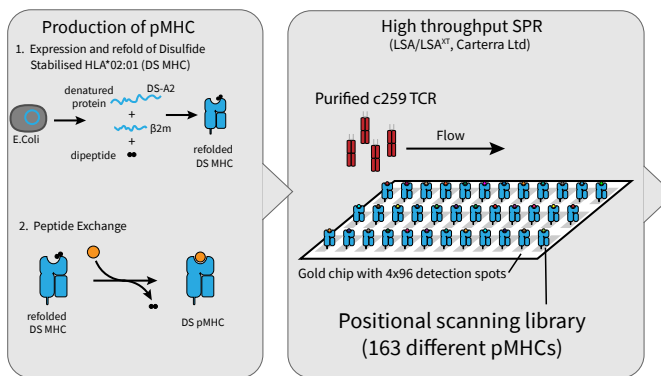


Figure S 7: High-throughput measurements of c259 TCR affinities with the 163 pMHCs from the positional scanning library by SPR at 37°C

Figure S7: **(A)** Schematic of high-throughput SPR workflow. Step 1: Production of pMHCs presenting peptides from the positional scanning peptide library. Disulfide-stabilised HLA-A*02:01 (DS-A2) and β 2m are expressed in *E.coli* as denatured protein chains, then refolded with a dipeptide. The dipeptide is exchanged with a peptide from the positional scanning peptide library by incubation. Step 2: High-throughput SPR setup. Using the LSA or LSA^{XT} instrument (Carterra) a pMHC carrying each peptide from the library is immobilised in a separate detection spot on the chip. Soluble TCR is injected and flows over the entire chip. Step 3: Acquisition of SPR sensograms. Each detection spot simultaneously measures TCR binding over time for each peptide from the peptide library. Step 4: Calculation of affinity values. The steady-state binding response is plotted over TCR concentration to calculate K_D values using the constrained Bmax methods optimised for measuring ultra-low TCR/pMHC affinities (22). Step 5: The mean K_D values as heat map. **(B)** The K_D determined using the Carterra LSA/LSA^{XT} instruments agrees favourably with the K_D values determined using a standard BIAcore (T200). **(C)** The K_D determined using the disulfide-stabilised MHC agrees favourably with the K_D determined using wild-type MHC for different peptides that bind the c259 TCR with a wide range of affinities.

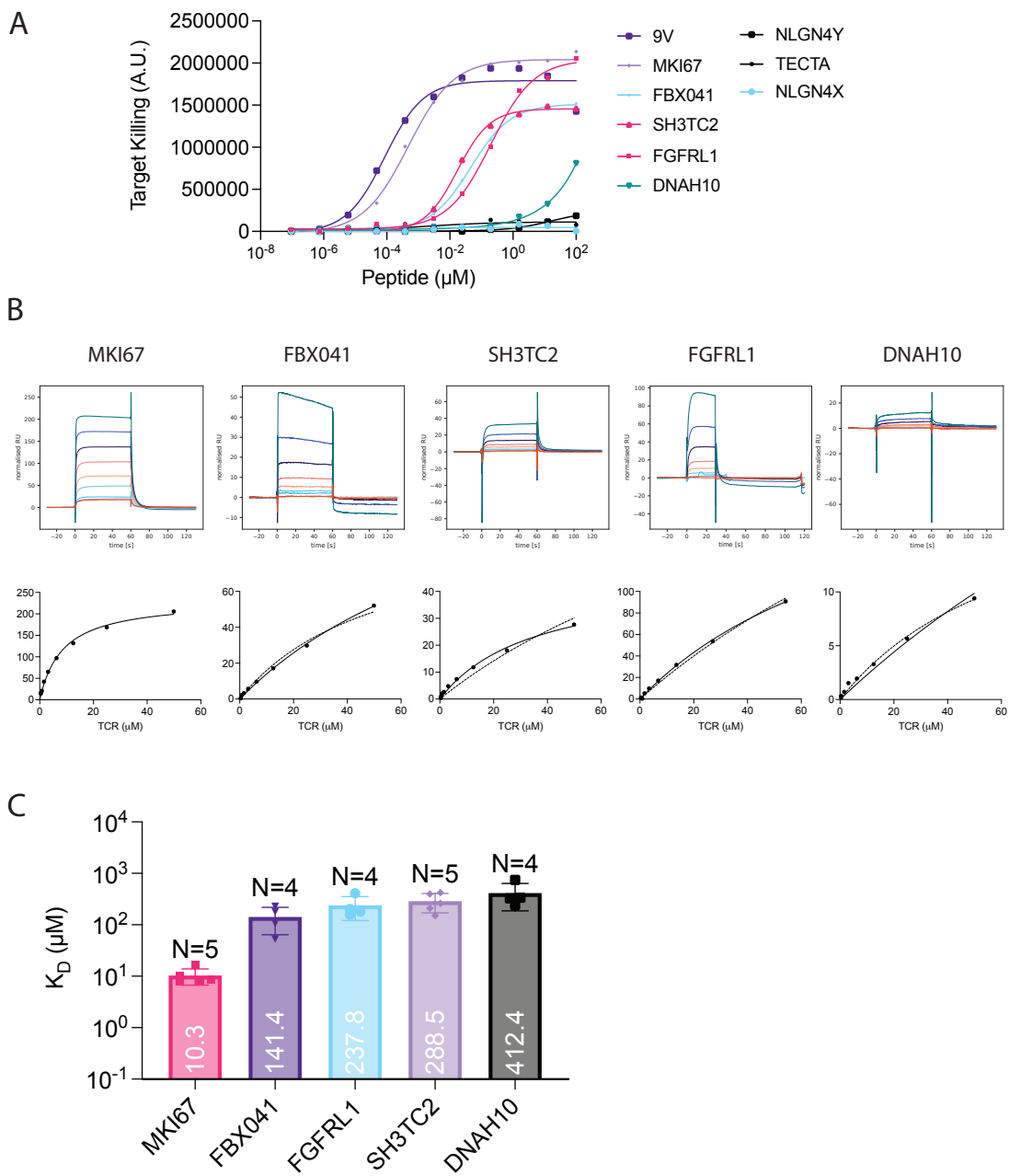


Figure S8: The c259 TCR affinity with a panel of self peptides measured by SPR at 37°C. (A) to stimulate WT c259 TCR-T cells. Target cell killing was measured after 20 hours. (B) The binding affinity of the c259 TCR to the peptides that induced T cell activation were measured. (Top) Representative SPR sensograms depicting injections of increasing concentrations of the c259 TCR. (Bottom) Representative equilibrium curves of c259 TCR binding to different self pMHCs. The TCR/pMHC affinity was calculated by constraining Bmax (dashed line) or fitting Bmax (solid line). (C) Steady-state binding affinity for the selected peptides. Barplot represents mean $K_D \pm \text{SDs}$. The affinities were calculated by constraining Bmax to the value obtained from the standard curve in (B) based on the amount of BBM.1 antibody that bound the chip surface (see Methods for details). All data fitting was performed using a one site-specific binding model in GraphPad Prism.

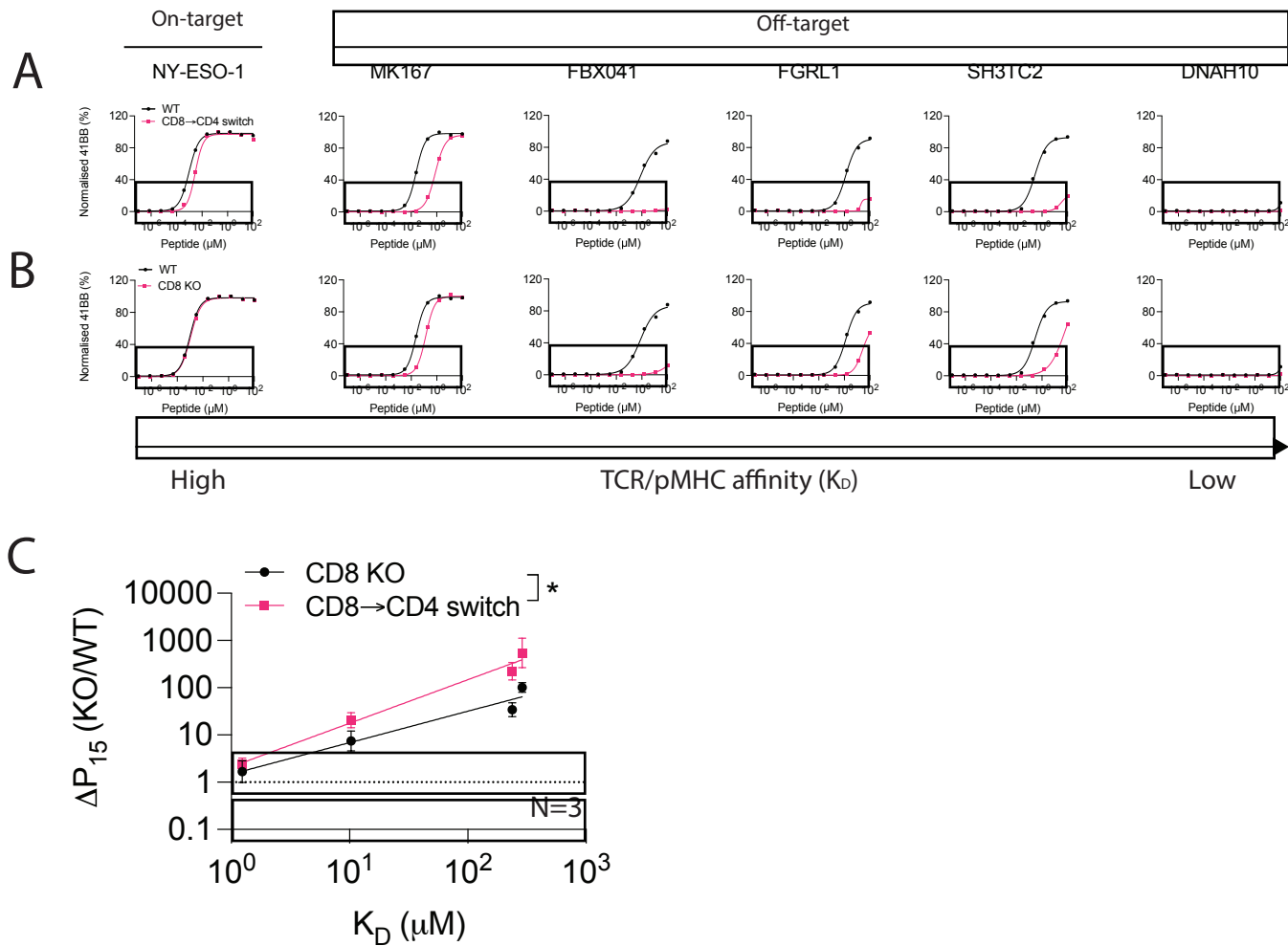


Figure S9: CD8→CD4 co-receptor switch cytotoxic display reduced activation against predicted self-peptides (4-1BB). (A) U87 cells were titrated with each of the predicted self-peptides to stimulate WT or CD8 KO cytotoxic c259 TCR-T cells. 4-1BB expression was measured after 20 hours. (B) U87 cells were titrated with each of the predicted self-peptides to stimulate WT or CD8→CD4 co-receptor switch cytotoxic c259 TCR-T cells. 4-1BB expression was measured after 20 hours. (C) Fold change in potency (P15) between modified or WT T cells from (A and B) is plotted over TCR/pMHC affinity (K_D). Data is shown as means ± SDs. Data in (A) and (B) are representative of N=3 independent experiments with different blood donors. P values were determined by an F-test. *p<0.05.

499 **Supplementary Tables**

Table S1: The c259 TCR affinities to the NY-ESO-1 peptide variants.

Abbr	Sequence	Mean	SD	N
9V	SLLMWITQV	1.240	0.129	3
6V	SLLMWVTQV	3.538	0.283	2
3Y	SLYMWITQV	10.350	1.634	4
6T	SLLMWTTQV	27.628	4.598	11
4D	SLLDWITQV	41.777	4.703	7
4A	SLLAWITQV	62.319	10.313	8
5Y	SLLMYITQV	157.666	23.818	3

Table S2: The c259 TCR affinities to the positional scanning peptide library. Geometric mean, geometric standard deviation across N experiments is reported. K_D values have been excluded if pMHC was unstable (indicated as N/A) or no TCR binding response was observed (indicated as NB).

Position 1					Position 2					Position 3				
Abbr	Sequence	Geo. mean	Geo. SD	N	Abbr	Sequence	Geo. mean	Geo. SD	N	Abbr	Sequence	Geo. mean	Geo. SD	N
1A	ALLMWITQV	2.606	2.781	2	2A	SALMWITQV	N/A			3A	SLAMWITQV	0.596	1.057	2
1D	DLLMWITQV	18.846	1	1	2D	SDLMWITQV	N/A			3D	SLDMWITQV	N/A		
1E	ELLMWITQV	N/A			2E	SELMWITQV	N/A			3E	SLEMWITQV	N/A		
1F	FLLMWITQV	57.473	5.281	2	2F	SFLMWITQV	N/A			3F	SLFMWITQV	13.441	3.048	3
1G	GLLMWITQV	3.478	3.361	3	2G	SGLMWITQV	N/A			3G	SLGMWITQV	N/A		
1H	HLLMWITQV	21.339	10.308	3	2H	SHLMWITQV	N/A			3H	SLHMWITQV	17.216	18.519	2
1I	ILLMWITQV	2.787	6.294	3	2I	SILMWITQV	5.397	63.1	2	3I	SLIMWITQV	6.639	11.558	3
1K	KLLMWITQV	1.444	8.647	3	2K	SKLMWITQV	N/A			3K	SLKMWITQV	N/A		
1L	LLLMWITQV	3.7	9.695	3	2L	SLLMWITQV	0.701	1.966	3	3L	SLLMWITQV	0.701	1.966	3
1M	MLLMWITQV	N/A			2M	SMLMWITQV	6.684	23.015	2	3M	SLMMWITQV	2.885	3.632	3
1N	NLLMWITQV	0.409	1	1	2N	SNLMWITQV	N/A			3N	SLNMWITQV	3.951	19.691	2
1P	PLLMWITQV	N/A			2P	SPLMWITQV	N/A			3P	SLPMWITQV	N/A		
1Q	QLLMWITQV	0.309	1.403	2	2Q	SQLMWITQV	2.241	14.094	2	3Q	SLQMWITQV	0.688	6.074	2
1R	RLLMWITQV	0.226	1.082	2	2R	SRLMWITQV	N/A			3R	SLRMWITQV	N/A		
1S	SLLMWITQV	0.701	1.966	3	2S	SSLMWITQV	N/A			3S	SLSMWITQV	1.82	2.026	3
1T	TLLMWITQV	1.046	3.568	2	2T	STLMWITQV	N/A			3T	SLTMWITQV	6.228	1	1
1V	VLLMWITQV	0.91	1.746	3	2V	SVLMWITQV	50.287	1	1	3V	SLVMWITQV	2.657	1	1
1W	WLLMWITQV	11.631	1.329	3	2W	SWLMWITQV	33.447	3.481	3	3W	SLWMWITQV	9.861	1.691	3
1Y	YLLMWITQV	3.993	1.292	3	2Y	SYLMWITQV	18.095	1.288	3	3Y	SLYMWITQV	15.39	1.34	3
Position 4					Position 5					Position 6				
Abbr	Sequence	Geo. mean	Geo. SD	N	Abbr	Sequence	Geo. mean	Geo. SD	N	Abbr	Sequence	Geo. mean	Geo. SD	N
4A	SLLAWITQV	431.199	19.596	2	5A	SLLMAITQV	450.833	2.219	2	6A	SLLMWATQV	46.1	1.912	3
4D	SLLDWITQV	55.894	4.407	3	5D	SLLMDITQV	1779.52	1	1	6D	SLLMWDTQV	226.549	1.541	2
4E	SLLEWITQV	335.407	3.105	3	5E	SLLMEITQV	406.72	2.54	3	6E	SLLMWETQV	971.245	1.531	2
4F	SLLFWITQV	248.389	1.439	3	5F	SLLMFITQV	730.463	1.622	3	6F	SLLMWFTQV	16.258	4.03	3
4G	SLLGWITQV	111.398	2.492	3	5G	SLLMGITQV	658.784	1.293	2	6G	SLLMWGTQV	118.893	1	1
4H	SLLHWITQV	161.301	1.704	3	5H	SLLMHITQV	1436.123	1	1	6H	SLLMWHTQV	61.979	1.624	3
4I	SLLIWITQV	85.441	1.52	3	5I	SLLMIITQV	220.473	1	1	6I	SLLMWITQV	0.701	1.966	3
4K	SLLKWITQV	22.035	4.9	3	5K	SLLMKITQV	654.509	2.109	2	6K	SLLMWKTQV	476.51	1.479	3
4L	SLLLWITQV	2.392	17.993	3	5L	SLLMLITQV	815.925	1.446	3	6L	SLLMWLTQV	5.596	5.279	3
4M	SLLMWITQV	0.701	1.966	3	5M	SLLMMITQV	670.428	1.447	2	6M	SLLMWMTQV	16.572	16.638	3
4N	SLLNWITQV	26.905	2.998	3	5N	SLLMNITQV	758.195	1	1	6N	SLLMWNTQV	40.021	2.134	3
4P	SLLPWITQV	241.083	2.6	3	5P	SLLMPITQV	N/A			6P	SLLMWPTQV	41.366	1	1
4Q	SLLQWITQV	0.927	1.821	3	5Q	SLLMQITQV	154.879	1	1	6Q	SLLMWQTQV	38.707	1.705	3
4R	SLLRWITQV	604.902	1.555	2	5R	SLLMRITQV	4576.089	1	1	6R	SLLMWRTQV	389.248	1.019	2
4S	SLLSWITQV	48.243	1.186	3	5S	SLLMSITQV	289.89	1.941	3	6S	SLLMWSTQV	12.323	2.107	3
4T	SLLTWITQV	2.985	1.985	3	5T	SLLMTITQV	584.582	1.56	3	6T	SLLMWTTQV	15.427	1.101	3
4V	SLLVWITQV	30.833	1.08	2	5V	SLLMVITQV	1048.028	1.686	2	6V	SLLMWVTQV	1.796	1.671	3
4W	SLLWWITQV	146.053	1.285	3	5W	SLLMWITQV	0.701	1.966	3	6W	SLLMWWTQV	9.808	1.354	3
4Y	SLLYWITQV	208.894	1.518	3	5Y	SLLMYITQV	243.945	1.92	3	6Y	SLLMWYTQV	12.347	1.439	3
Position 7					Position 8					Position 9				
Abbr	Sequence	Geo. mean	Geo. SD	N	Abbr	Sequence	Geo. mean	Geo. SD	N	Abbr	Sequence	Geo. mean	Geo. SD	N
7A	SLLMWIAQV	15.201	3.121	3	8A	SLLMWITAV	126.651	3.221	3	9A	SLLMWITQA	6.31	18.975	3
7D	SLLMWIDQV	6.163	9.833	3	8D	SLLMWITDV	440.519	1.688	2	9D	SLLMWITQD	N/A		
7E	SLLMWIEQV	85.179	1.266	3	8E	SLLMWITEV	1758.587	2.616	3	9E	SLLMWITQE	N/A		
7F	SLLMWIFQV	408.909	1.802	3	8F	SLLMWITFV	961.039	1	1	9F	SLLMWITQF	1773.142	1	1
7G	SLLMWIGQV	65.685	9.19	2	8G	SLLMWITGV	45.631	3.139	3	9G	SLLMWITQG	N/A		
7H	SLLMWIHQV	45.044	4.503	3	8H	SLLMWITHV	99.112	1.372	3	9H	SLLMWITQH	N/A		
7I	SLLMWIIHQV	168.64	2.155	3	8I	SLLMWITIV	267.092	1.481	2	9I	SLLMWITQI	51.817	1	1
7K	SLLMWIKQV	259.139	1	1	8K	SLLMWITKV	305.156	1.099	2	9K	SLLMWITQK	N/A		
7L	SLLMWILQV	321.614	1.129	2	8L	SLLMWITLV	357.078	2.024	2	9L	SLLMWITQL	3.39	1.913	2
7M	SLLMWIMQV	127.392	2.346	3	8M	SLLMWITMV	536.124	1.767	3	9M	SLLMWITQM	N/A		
7N	SLLMWINQV	20.053	7.134	3	8N	SLLMWITNV	N/A			9N	SLLMWITQN	N/A		
7P	SLLMWIPQV	83.799	4.303	3	8P	SLLMWITPV	N/A			9P	SLLMWITQP	N/A		
7Q	SLLMWIQQV	58.27	1.297	3	8P	SLLMWITQV	0.701	1.966	3	9Q	SLLMWITQQ	4607.455	1	1
7R	SLLMWIRQV	738.23	1.616	2	8R	SLLMWITRV	109.572	1.42	3	9R	SLLMWITQR	N/A		
7S	SLLMWISQV	1.199	1.839	3	8S	SLLMWITSV	122.849	1.544	3	9S	SLLMWITQS	N/A		
7T	SLLMWITQV	0.701	1.966	3	8T	SLLMWITTV	420.7	2.238	3	9T	SLLMWITQT	N/A		
7V	SLLMWIVQV	196.983	2.279	3	8V	SLLMWITVV	330.714	5.072	2	9V	SLLMWITQV	0.701	1.966	3
7W	SLLMWIWQV	1497.217	4.298	2	8W	SLLMWITWV	677.351	3.87	3	9W	SLLMWITQW	88.229	1	1
7Y	SLLMWIYQV	1190.897	2.148	3	8Y	SLLMWITYV	129.924	3.947	2	9Y	SLLMWITQY	N/A		

Table S3: The c259 TCR affinities to predicted self-peptides.

Gene	Sequence	Mean	SD	N
NY-ESO-1 (9V)	SLLMWITQV	1.240	0.129	3
MKI67	FLTLWLTQV	10.314	3.612	5
FBX041	MLAQWCTQA	141.35	60.426	4
FGFRL1	TLLLWLCQA	237.775	116.323	4
SH3TC2	QVFLWLAQV	288.480	117.831	5
DNAH10	CVINWLNI	412.425	225.050	4